Electronic Supplementary Information

Teaching indicators to unravel the kinetic features of host-guest inclusion complexes

Amrutha Prabodh,[a] Stephan Sinn,*[a] Laura Grimm,[a] Zsombor Miskolczy,[b] Mónika Megyesi,[b] László Biczók,[b] Stefan Bräse,[c] and Frank Biedermann*[a]

a Dr. S. Sinn, MSc. A. Prabodh, MSc. L. Grimm, Dr. F. Biedermann
Institute of Nanotechnology (INT)
Karlsruhe Institute of Technology (KIT),
Hermann-von-Helmholtz Platz 1, 76344 Eggenstein-Leopoldshafen
Germany
E-Mail: stephan.sinn@kit.edu
E-Mail:frank.biedermann@kit.edu

b Dr. Z. Miskolczy, Dr. M. Megyesi, Prof. L. Biczók
Institute of Materials and Environmental Chemistry
Research Centre for Natural Sciences
Magyar tudósok körútja 2, 1117 Budapest, Hungary

c Prof. Dr. S. Bräse
Institute of Organic Chemistry (IOC)
Karlsruhe Institute of Technology (KIT)
Fritz-Haber-Weg 6, 76131 Karlsruhe (Germany)
Inst. f. Biologische und Chemische Systeme - Funktionelle molekulare Systeme (IBCS-FMS)
Hermann-von-Helmholtz Platz 1, 76344 Eggenstein-Leopoldshafen
&
Karlsruhe Institute of Technology (KIT)
Institute of Toxicology and Genetics (ITG)
Hermann-von-Helmholtz-Platz 1
76344 Eggenstein-Leopoldshafen, (Germany).

1 Table of Contents

2 General Information

2.1 Abbreviations

H	host
G	guest
D	(indicator) dye
DBA	direct-binding assay
*kin*DBA	kinetic DBA
IDA	indicator-displacement assay
*kin*IDA	kinetic IDA
GDA	guest-displacement assay
*kin*GDA	kinetic GDA
*kin*GDA^{PFO}	pseudo-first order *kin*GDA
CB6	cucurbit[6]uril
CB8	cucurbit[8]uril
CB7	cucurbit[7]uril
HSA	human serum albumin (fatty acid free)
DSMI	*trans*-4-[4-(Dimethylamino)styryl]-1-methylpyridinium iodide
BE	berberine
MDAP	*N,N'*-dimethyl diazapyrene
MPCP	(*rac*)-*N*-methyl-4-pyridinylium[2.2]paracyclophane
MV	methyl viologen (doubly oxidized form, 2+)
4-MBA	4-methylbenzylamine hydrochloride
AdOH	1-adamantanol
$FeCp_2OH$	ferrocenyl methanol
PBZ	phenylbutazone
PB	sodium phosphate buffer
PBS	phosphate buffered saline (137 mM NaCl, 2.7 mM KCl, 10 mM Na_2HPO_4 and 2 mM KH_2PO_4 dissolved in water)
NMR	nuclear magnetic resonance
ITC	isothermal titration calorimetry
λ	wavelength
ε	molar extinction coefficient
I	observable signal (fluorescence intensity)

2.2 Solubility

Table S1: Solubility of selected guests in water

compound	solubility in water	reference
1-adamantanol	soluble (> 2 mM)	[1]
PBZ (aq. solution)	145 µM	[2]
nandrolone	810 µM	[3]
testosterone	114 µM	[3]
prednisolone	483 µM	[3]
estradiol	9 µM	[3]
progesterone	33 µM	[3]
warfarin (aq. solution)	55.1 µM	[4]
berberine chloride	13.2 mM	[5]
methyl viologen	2.50 M	[6]
(+)-fenchone	14.1 mM	[7]
norcamphor	264 mM	[8]

2.3 Photophysical properties

Table S2: Photophysical properties of used dyes and corresponding host:dye complexes

dye	host	λ_{abs}^{max} / nm[a]	λ_{em}^{max} / nm[b]
DSMI	–	450	596
	CB6	450	575
BE	–	432	540 [c]
	CB7	430	500
MDAP	–	416	425
	CB7	423	431
MPCP	–	335	535
	CB8	342	542
warfarin[d]	–	308	402
	HSA	308	391

If not stated differently all measurements were conducted in deionized water at 25°C. [a] maximum of the lowest-energy band. [b] maximum of the highest-energy band. [c] almost no emission signal detectable. [d] measured in PBS.

2.4 Experimental details

All solvents were used as received from Aldrich or Fluka without any further purification and all chemicals were used as received from the manufacturer, if not stated otherwise. ^{1}H NMR spectra were recorded on a Bruker Avance 500 spectrometer. The ^{1}H NMR chemical shifts (δ) are given in ppm and refer to residual protons on the corresponding deuterated solvent. All deuterated solvents were used as received without any further purification. All coupling constants (J) are given in Hertz (Hz).

Absorption spectra were measured on a Jasco V-730 double-beam or on an Agilent Technologies Cary60 UV–Vis spectrophotometer and baseline corrected. Steady-state emission spectra and time resolved emission profiles were recorded on a Jasco FP-8300 fluorescence spectrometer equipped with a 450 W xenon arc lamp, double-grating excitation, emission monochromators or on a Jobin-Yvon Fluoromax-P spectrofluorometer. Emission spectra were corrected for source intensity (lamp and grating) and the emission spectral response (detector and grating) by standard correction curves. For spectral recording the automatic filter change of the FP-8300 was applied in order to exclude second order diffraction artefacts. All kinetic experiments were carried out at T=25°C by using a water thermostated cell holder STR-812, while the cuvettes were equipped with a stirrer allowing rapid mixing. Stopped-flow experiments were carried out on a Jasco FP-8300 fluorescence spectrometer equipped with a thermostated (25°C) SFA-20 stopped-flow accessory from TgK Scientific Limited or on a Jobin-Yvon Fluoromax-P spectrofluorometer using a thermostated Applied Photophysics RX2000 rapid mixing accessory, which were driven by pneumatic drives. For UV-Vis absorption experiments UV plastic cuvettes with a light path of 10 mm and dimensions of 10x10 mm from Brand with a spectroscopic cut-off at 240 nm were utilized. For fluorescence-based kinetics experiments, PMMA cuvettes with a light path of 10 mm and dimensions of 10x10 mm from Brand with a spectroscopic cut-off at 300 nm were utilized.

The ITC experiments were carried out on a Microcal PEAQ-ITC from Malvern. All spectral experiments were conducted under air at room temperature, in Millipore H_2O or in H_2O freshly distilled three times from dilute $KMnO_4$ solution. During titrations, all concentrations were kept constant except for that of the titrant. All data were baseline corrected by the average value of the titration curve of guest into water.

The differential equations describing the kinetic processes presented in the paper have been solved numerically with Wolfram Mathematica 11/12. An analytical solution might be also possible by Laplace transformations.[9, 10]

3 Mathematical Equations for Kinetic Assay

3.1 Direct–Binding Assay (*kin*DBA)

$$\mathrm{H} + \mathrm{D} \underset{k_{\mathrm{out}}^{\mathrm{HD}}}{\overset{k_{\mathrm{in}}^{\mathrm{HD}}}{\rightleftarrows}} \mathrm{HD} \qquad \text{Eq. S1}$$

$$\frac{\mathrm{d}[\mathrm{HD}]_t}{\mathrm{d}t} = k_{\mathrm{in}}^{\mathrm{HD}} \cdot [\mathrm{H}]_t[\mathrm{D}]_t - k_{\mathrm{out}}^{\mathrm{HD}} \cdot [\mathrm{HD}]_t \qquad \text{Eq. S2}$$

$$\frac{\mathrm{d}[\mathrm{D}]_t}{\mathrm{d}t} = -k_{\mathrm{in}}^{\mathrm{HD}} \cdot [\mathrm{H}]_t[\mathrm{D}]_t + k_{\mathrm{out}}^{\mathrm{HD}} \cdot [\mathrm{HD}]_t \qquad \text{Eq. S3}$$

$$\frac{\mathrm{d}[\mathrm{H}]_t}{\mathrm{d}t} = -k_{\mathrm{in}}^{\mathrm{HD}} \cdot [\mathrm{H}]_t[\mathrm{D}]_t + k_{\mathrm{out}}^{\mathrm{HD}} \cdot [\mathrm{HD}]_t \qquad \text{Eq. S4}$$

$$I_t = I^0 + I^{\mathrm{HD}} \cdot [\mathrm{HD}]_t + I^{\mathrm{D}} \cdot [\mathrm{D}]_t \qquad \text{Eq. S5}$$

$[H]_t$ – host concentration at time t, $[D]_t$ – dye concentration at time t,
$[HD]_t$ – host⊃dye concentration at time t,
k_{in}^{HD} – rate constant for the association of the host⊃dye (HD) complex (complexation),
k_{out}^{HD} – rate constant for the dissociation of the host⊃dye (HD) complex (decomplexation),
I^0 – background signal, I^{HD} – constant proportional to the fluorescence efficiency of host⊃dye (HD) complex at the monitoring wavelength, I^D – constant proportional to the fluorescence efficiency of free dye (D) at the monitoring wavelength,
I_t – observable signal as a function of time

3.2 Guest–Displacement & Indicator-Displacement Assay (*kin*GDA & *kin*IDA)

$$\mathrm{HG} + \mathrm{D} \rightleftarrows \mathrm{HD} + \mathrm{G} \qquad \text{Eq. S6}$$

$$\mathrm{H} + \mathrm{G} \underset{k_{\mathrm{out}}^{\mathrm{HG}}}{\overset{k_{\mathrm{in}}^{\mathrm{HG}}}{\rightleftarrows}} \mathrm{HG} \qquad \text{Eq. S7}$$

$$\mathrm{H} + \mathrm{D} \underset{k_{\mathrm{out}}^{\mathrm{HD}}}{\overset{k_{\mathrm{in}}^{\mathrm{HD}}}{\rightleftarrows}} \mathrm{HD} \qquad \text{Eq. S8}$$

$$\frac{\mathrm{d}[\mathrm{HD}]_t}{\mathrm{d}t} = k_{\mathrm{in}}^{\mathrm{HD}} \cdot [\mathrm{H}]_t[\mathrm{D}]_t - k_{\mathrm{out}}^{\mathrm{HD}} \cdot [\mathrm{HD}]_t \qquad \text{Eq. S9}$$

$$\frac{\mathrm{d}[\mathrm{D}]_t}{\mathrm{d}t} = -k_{\mathrm{in}}^{\mathrm{HD}} \cdot [\mathrm{H}]_t[\mathrm{D}]_t + k_{\mathrm{out}}^{\mathrm{HD}} \cdot [\mathrm{HD}]_t \qquad \text{Eq. S10}$$

$$\frac{\mathrm{d}[\mathrm{HG}]_t}{\mathrm{d}t} = k_{\mathrm{in}}^{\mathrm{HG}} \cdot [\mathrm{H}]_t[\mathrm{G}]_t - k_{\mathrm{out}}^{\mathrm{HG}} \cdot [\mathrm{HG}]_t \qquad \text{Eq. S11}$$

$$\frac{\mathrm{d}[\mathrm{G}]_t}{\mathrm{d}t} = -k_{\mathrm{in}}^{\mathrm{HG}} \cdot [\mathrm{H}]_t[\mathrm{G}]_t + k_{\mathrm{out}}^{\mathrm{HG}} \cdot [\mathrm{HG}]_t \qquad \text{Eq. S12}$$

$$\frac{\mathrm{d}[\mathrm{H}]_t}{\mathrm{d}t} = -k_{\mathrm{in}}^{\mathrm{HD}} \cdot [\mathrm{H}]_t[\mathrm{D}]_t + k_{\mathrm{out}}^{\mathrm{HD}} \cdot [\mathrm{HD}]_t - k_{\mathrm{in}}^{\mathrm{HG}} \cdot [\mathrm{H}]_t[\mathrm{G}]_t + k_{\mathrm{out}}^{\mathrm{HG}} \cdot [\mathrm{HG}]_t \qquad \text{Eq. S13}$$

$$I_t = I^0 + I^{\mathrm{HD}} \cdot [\mathrm{HD}]_t + I^{\mathrm{D}} \cdot [\mathrm{D}]_t \qquad \text{Eq. S14}$$

$[H]_t$ – host concentration at time t, $[D]_t$ – dye concentration at time t,
$[G]_t$ – guest concentration at time t, $[HD]_t$ – host⊃dye concentration at time t,
$[HG]_t$ – host⊃guest concentration at time t,
k_{in}^{HD} – rate constant for the association of the host⊃dye (HD) complex (complexation),
k_{out}^{HD} – rate constant for the dissociation of the host⊃dye (HD) complex (decomplexation),
k_{in}^{HG} – rate constant for the association of the host⊃guest (HG) complex (complexation),
k_{out}^{HG} – rate constant for the dissociation of the host⊃guest(HG) complex (decomplexation),
I^0 – background signal, I^{HD} – constant proportional to the fluorescence efficiency of host⊃dye (HD) complex at the monitoring wavelength, I^D – constant proportional to the fluorescence efficiency of free dye (D) at the monitoring wavelength,
I_t – observable signal as a function of time

3.3 GDA – Pseudo First Order (*kin*GDA^{PFO})

$$k_{\text{in}}^{\text{HG}}\,[\text{G}]_0 \ll k_{\text{in}}^{\text{HD}}\,[\text{D}]_0 \qquad \text{Eq. S15}$$

$$\text{HG} + \text{D} \xrightarrow{k_{\text{out}}^{\text{HG}}} \text{H} + \text{G} + \text{D} \xrightarrow{k_{\text{in}}^{\text{HD}}} \text{HD} + \text{G} \qquad \text{Eq. S16}$$

$$k_{\text{out}}^{\text{HG}} \ll k_{\text{in}}^{\text{HD}}[\text{D}]_0 \qquad \text{Eq. S17}$$

$$\text{HG} + \text{D} \xrightarrow{k_{\text{out}}^{\text{HG}}} \text{HD} + \text{G} \qquad \text{Eq. S18}$$

$$\frac{\text{d}[\text{HD}]_t}{\text{dt}} = -\frac{\text{d}[\text{HG}]_t}{\text{dt}} = k_{\text{out}}^{\text{HG}} \cdot [\text{HG}]_t \qquad \text{Eq. S19}$$

$$\frac{\text{d}[\text{HG}]_t}{[\text{HG}]_t} = -k_{\text{out}}^{\text{HG}} \cdot \text{d}t \qquad \int_{[\text{HG}]_0}^{[\text{HG}]_t} \frac{\text{d}[\text{HG}]_t}{[\text{HG}]_t} = \int_0^t -k_{\text{out}}^{\text{HG}} \cdot \text{d}t \qquad \text{Eq. S20}$$

$$\ln[\text{HG}]_t = \ln[\text{HG}]_0 - k_{\text{out}}^{\text{HG}} \cdot t \qquad [\text{HG}]_t = [\text{HG}]_0\, e^{-k_{\text{out}}^{\text{HG}} \cdot t} \qquad \text{Eq. S21}$$

$$I_t = I^{eq.} + Ae^{-k_{\text{out}}^{\text{HG}} \cdot t} \qquad \text{Eq. S22}$$

$[D]_t$ – dye concentration at time t, $[D]_0$ – dye concentration at time 0 (initial dye concentration),
$[G]_t$ – guest concentration at time t,
$[G]_0$ – guest concentration at time 0 (initial guest concentration),
$[HD]_t$ – host⊃dye concentration at time t,
$[HG]_t$ – host⊃guest concentration at time t,
$[HG]_0$ – host⊃guest concentration at time 0 (preequilibrated host⊃guest complex),
k_{in}^{HD} – rate constant for the association of the host⊃dye (HD) complex (complexation),
k_{out}^{HD} – rate constant for the dissociation of the host⊃dye (HD) complex (decomplexation),
k_{in}^{HG} – rate constant for the association of the host⊃guest (HG) complex (complexation),
k_{out}^{HG} – rate constant for the dissociation of the host⊃guest(HG) complex (decomplexation),
$I^{eq.}$ – signal offset (at equilibration of HD), A – amplitude,
I_t – observable signal as a function of time

4 Determination of Kinetic Constants

4.1 Best Practice Guide for *kin*GDA and *kin*GDA^{PFO}

1. Gather information on solubility of host and guest in solvent of interest.
2. Estimate binding constant and kinetic rate constants of host-guest complex, e.g. by searching for related host-guest pairs on www.suprabank.org, www.supramolecular.org or in reviews.
3. Calculate which concentration of host and guest are needed to reach a sufficient degree of complexation of host (ideally ≥ 50%[11]). A software package is available from the authors upon request and provided on GitHub: https://github.com/ASDSE/thermosimfit/zipball/master for simulations. Excess of guest is permitted for *kin*GDA and *kin*IDA. If required guest concentration is within the solubility window, continue with step 5.
4. If required guest concentration is outside the solubility window, attempt to solubilize the guest in a solution of the host (sonication can help), followed by filtration/centrifugation and concentration determination of the host and guest concentration (e.g. by NMR, UV-Vis, HPLC etc., see section 6)
5. Simulate *kin*GDA by using Eq. S14 and adjust the indicator concentration and the host-guest concentration, while maintaining the degree of host-complexation sufficiently high. (A software package is available from the authors upon request and provided on GitHub: https://github.com/ASDSE/kineticsimfit/zipball/master for simulations.) Consider the solubility limit of the indicator. Ideally, dyes that show stronger emission or distinct absorbance spectra upon host binding are chosen.
6. Simulate the *kin*DBA (without guest) and *kin*GDA (with guest) for comparison. The *kin*GDA and *kin*DBA kinetic traces should look sufficiently distinct, if not, choose different concentrations or a different indicator dye.
7. Perform the *kin*GDA with the conditions derived from the simulations by rapidly mixing the pre-equilibrated H⊃G solution with the dye solution at a controlled temperature. Practically, equilibration time should be ≥ 100 ms for conventional stopped-flow setups. If equilibration times are ≥ 1 min manual mixing may be used.
8. Fit the recorded *kin*GDA traces by using equations Eq. S14 utilizing the predetermined parameters: $K_a^{HD}, k_{in}^{HD}, k_{out}^{HD}$ and the exact concentrations as an input. Utilizing $k_{in}^{HG} = k_{out}^{HG} \cdot K_a^{HG}$ as an input will increase the goodness of the fit. (A software package is available from the authors upon request and provided on GitHub: https://github.com/ASDSE/kineticsimfit/zipball/master for fitting.) The signal factors I^{HD} and I^{D} may be varied but their ratio should

stay close to the expected value from the host-dye titration experiment. From the fitting, the host-guest kinetic rate constants $k_{in}^{HG}, k_{out}^{HG}$ can be extracted. Analogously, this procedure can be applied for the akin method of *kin*IDA.

9. For *kin*GDA^{PFO} perform steps 1 – 7, but with a large excess of dye. Fit the acquired kinetic traces to Eq. S22 to obtain k_{out}^{HG}. Subsequently, k_{in}^{HG} can be derived by using the relation $k_{in}^{HG} = k_{out}^{HG} \cdot K_a^{HG}$.

4.2 Error estimation

In order to provide a decent error estimation, up to seven repetition experiments were conducted at the exact same conditions. The estimated true value of the kinetic rate constant was then calculated by the arithmetic mean and compared to the median of the sample set. The resulting standard deviation was subsequently used to calculate the error based on a 95% confidence interval (CI) applying a t-distribution. In some cases, the number of repetitions was decreased for practical reasons (very long equilibration time). The t-distribution accounts for a reduced sampling size by the incorporated degrees-of-freedom.[11]

The error estimation is demonstrated for the *kin*GDA experiment of the guest nandrolone (=19-nortestosterone) (1.02 µM) with the host CB8 (1.01 µM) and MPCP (50 µM) as indicator in water. The affinity value $K_a = 1.12 \cdot 10^7\ M^{-1}$ was determined in a separate thermodynamic experiment under the same conditions. The results obtained for k_{in} (in $s^{-1}M^{-1}$) are:

$9.80 \cdot 10^6$	$1.08 \cdot 10^7$	$1.13 \cdot 10^7$	$1.13 \cdot 10^7$	$1.13 \cdot 10^7$	$1.13 \cdot 10^7$	$1.14 \cdot 10^7$

Mean =	$1.1 \cdot 10^7$	$s^{-1}M^{-1}$
StDev =	$5.74 \cdot 10^5$	$s^{-1}M^{-1}$
α =	5%	
CI =	95%	
DF =	6	
Error =	$5.31 \cdot 10^5$	$s^{-1}M^{-1}$
Error ~	5%	

Although the error typically is equal or lower than 10% for the competitive binding assays shown, the estimated errors of the direct binding assays for indicator and host have to be taken into account as well. Here we typically obtained a greater error between 10 – 30%. As the pseudo-first order *kin*GDA^{PFO} method is independent of the kinetic rate constants of the used (as long as complying to the prerequisites), this method is very precise. For the competitive methods *kin*GDA and *kin*IDA an error propagation (even on the basis of an analytical solution) is not trivial. We recommend to apply a larger error estimate of ≤ 30% as a save interval for the determined kinetic rate constants, which also covers lab-to-lab differences due to use of CB*n* specimens with different amounts and types of salts.

4.3 Binding Kinetics

Table S3: Kinetic constants for the analyzed guests with different hosts

guest	host	dye	k_{in}[a] / s^{-1} M^{-1}	k_{out}[a] / s^{-1}	method	log (K_a/M^{-1})
DSMI (0.27 µM)	CB6 (0.28 µM)	–	1.95 (± 0.8)·10^8	24.42 (± 0.4)	*kin*DBA	6.90
4-MBA[b] (8.23 µM)	CB6 (1.05 µM)	DSMI (2.08 µM)	3.33 (± 0.03)·10^4	6.49 (± 0.05)·10^{-4}	*kin*IDA	7.71
BE (0.23 µM)[c]	CB7 (0.23 µM)	–	1.9 (± 0.1) 10^7	0.81 (± 0.08)	*kin*DBA	7.38
BE (0.2 µM)	CB7 (0.3 µM)	–	6.0 (± 1.5)·10^6	0.4 (± 0.1)	*kin*DBA	7.23[h]
BE (1.2 µM)	CB7[d] (1 µM)	–	2.47 (± 0.3)·10^6	0.23 (± 0.03)	*kin*DBA	7.03
MDAP (71 nM)	CB7 (72 nM)	–	2.4 (± 0.5)·10^7	9.0 (± 1.8)·10^{-3}	*kin*DBA	9.43[h]
nandrolone (2 µM)	CB7 (2 µM)	BE[e] (50 µM)	3.0 (± 0.2)·10^3	3.7 (± 0.1)·10^{-2}	*kin*GDA^{PFO}	5.18[i]
		MDAP[e] (25 µM)	2.5 (± 0.1)·10^3	3.1 (± 0.1)·10^{-2}	*kin*GDA^{PFO}	5.18[i]
		BE (2 µM)	4.1 (± 0.4)·10^3	3.6 (± 0.2)·10^{-4}	*kin*GDA	7.05[j]
		BE (2 µM)	4.5 (± 0.3)·10^3	4.1 (± 0.2)·10^{-4}	*kin*IDA	7.05[j]
		BE (50 µM)	2.3 (± 0.4)·10^3	2.0 (± 0.2)·10^{-4}	*kin*GDA	7.05[j]
		BE (50 µM)	2.4 (± 0.5)·10^3	2.1 (± 0.2)·10^{-4}	*kin*GDA^{PFO}	7.05[j]
		MDAP (40 µM)	9.2 (± 0.2)·10^3	8.2 (± 0.8)·10^{-4}	*kin*GDA	7.05[j]
		MDAP (40 µM)	9.2 (± 0.2)·10^3	8.3 (± 0.8)·10^{-4}	*kin*GDA^{PFO}	7.05[j]
cholesterol[f] (2.5 µM)	CB7 (2.2 µM)	BE (50 µM)	7.0 (± 0.1)·10^4	8.7 (± 0.1)·10^{-2}	*kin*GDA	5.91[h]
			7.0 (± 0.1)·10^4	8.7 (± 0.1)·10^{-2}	*kin*GDA^{PFO}	5.91[h]
estradiol (3.9 µM)	CB7 (3.9 µM)		4.2 (± 0.1)·10^4	2.0 (± 0.1)·10^{-2}	*kin*GDA	6.25[h]
			4.3 (± 0.1)·10^4	2.1 (± 0.1)·10^{-2}	*kin*GDA^{PFO}	6.25[h]
AdOH (5 µM)	CB7[d] (1 µM)	BE (1.2 µM)	1.7 (± 0.1)·10^5	6.6 (± 0.4)·10^{-6}	*kin*IDA	10.41
(+)-fenchone (5.1 µM)	CB7 (0.25 µM)	BE[c] (2.5 µM)	9.2 (± 0.5) 10^4	3.2 (± 0.1) 10^{-3}	*kin*GDA	7.45
norcamphor (0.35 µM)	CB7 (0.25 µM)	BE[c] (32 µM)	1.5 (± 0.1) 10^7	9.8 (± 0.3) 10^{-2}	*kin*GDA	8.18
MPCP (0.2 µM)	CB8 (0.1 µM)		1.2 (± 0.6)·10^7	3.0 (± 1.6)·10^{-6}	*kin*DBA	12.59 [l]
MPCP (0.2 µM)	CB8[d] (0.2 µM)	–	2.0 (± 1.0)·10^7	5.1 (± 1.6)·10^{-6}	*kin*DBA	12.59 [l]
nandrolone (1 µM)	CB8 (1 µM)	MPCP (50 µM)	1.1 (± 0.1)·10^7	6.8 (± 0.4)·10^{-2}	*kin*GDA	8.19[h]
			1.1 (± 0.1)·10^7	7.1 (± 0.2)·10^{-2}	*kin*GDA^{PFO}	8.19[h]
prednisolone (5 µM)	CB8 (5 µM)	MPCP (50 µM)	1.6 (± 0.2)·10^6	1.1 (± 0.1)	*kin*GDA	6.15[j]
			1.5 (± 0.2)·10^6	1.1 (± 0.1)	*kin*GDA^{PFO}	6.15[j]
testosterone (5 µM)			6.4 (± 0.2)·10^5	5.8 (± 0.2)·10^{-3}	*kin*GDA	8.04[j]
			6.4 (± 0.2)·10^5	5.8 (± 0.2)·10^{-3}	*kin*GDA^{PFO}	8.04[ji]
$FeCp_2OH$ (0.8 µM)	CB8[d] (0.56 µM)	MPCP (5.25 µM)	2.08 (± 0.13)·10^7	5.77 (± 0.37)	*kin*GDA	6.56[k]
			2.04 (± 0.17)·10^7	5.67 (± 0.17)	*kin*GDA^{PFO}	6.56[k]
AdOH (1.4 µM)	CB8[d] (1 µM)	MPCP (10 µM)	1.22 (± 0.03)·10^7	1.97 (± 0.06)	*kin*GDA	6.79[k]
			1.22 (± 0.02)·10^7	1.92 (± 0.02)	*kin*GDA^{PFO}	6.79[k]
warfarin[g] (100 µM)	HSA (20 µM)	–	6.7 (± 0.9)·10^5	4.8 (± 0.6)	*kin*DBA	5.15[h]
phenylbutazone[g] (40µM)	HSA (20 µM)	warfarin (100 µM)	6.6 (± 0.6)·10^5	1.0 (± 0.1)	*kin*GDA	5.83[h]

If not stated differently all experiments have been conducted in deionized water at 25°C. [a] mean and standard deviation in parenthesis of at least 3 independent measurements. [b] in deionized water with 8.23 µM HCl. [c] BE was chromatographed on silica gel (Merck) column eluting with ethanol and water was freshly distilled three times from dilute $KMnO_4$ solution ref.[12] [d] desalted CB7/CB8 was used. [e] in sodium phosphate buffer (50 mM). [f] H_2O/ethanol (99.9/0.1; v/v) mixture. [g] in PBS. [h] ref.[13] [i] calculated using the formula presented in ref.[14] [j] ref.[3] [k] determined by ITC. [l] ref.[15]. Note: *kin*DBA were conducted at several concentrations of the dye, fitted to the DBA algorithm and kinetic rate constants averaged. The ESI comprises exemplified data.

4.3.1 CB6⊃DSMI

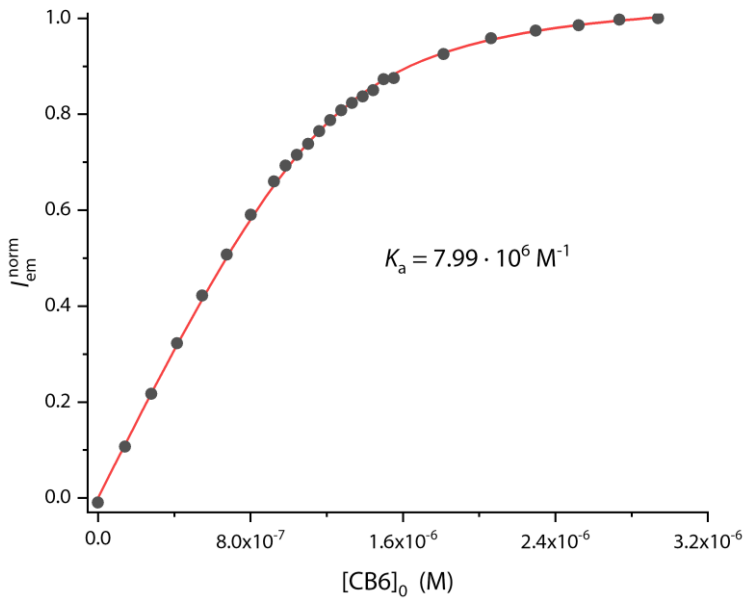

Fig. S1: Representative DBA binding isotherm determined by fluorescence intensity variations (λ_{exc} = 519 nm, λ_{em} = 575 nm) of DSMI (1.21 µM) and CB6 (0 – 2.94 µM) in water at 25°C. Acquired data is depicted as gray dots and fitted data as red line.

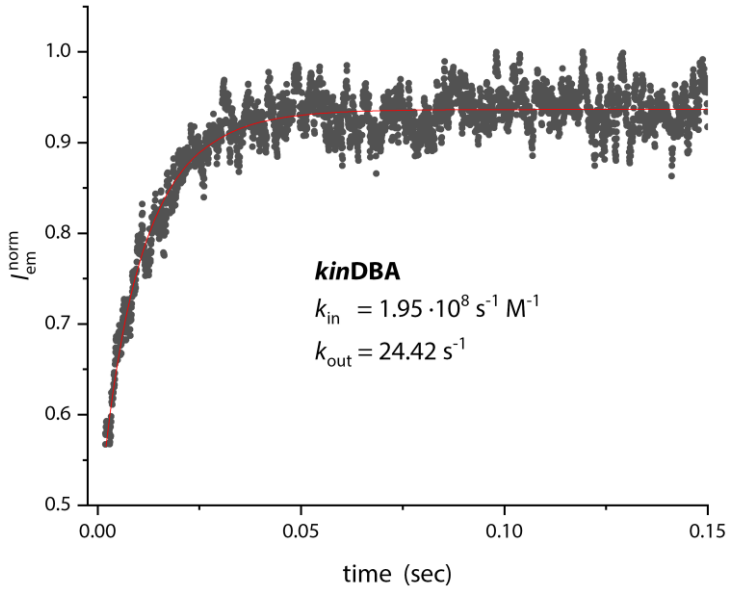

Fig. S2: Representative DBA kinetic binding curve determined by fluorescence intensity variations (λ_{exc} = 450 nm, λ_{em} = 575 nm) of DSMI (0.27 µM) and CB6 (0.28 µM) in water at 25°C. Acquired data are depicted as gray dots and fitted data as red line.

4.3.2 CB6⊃4-MBA

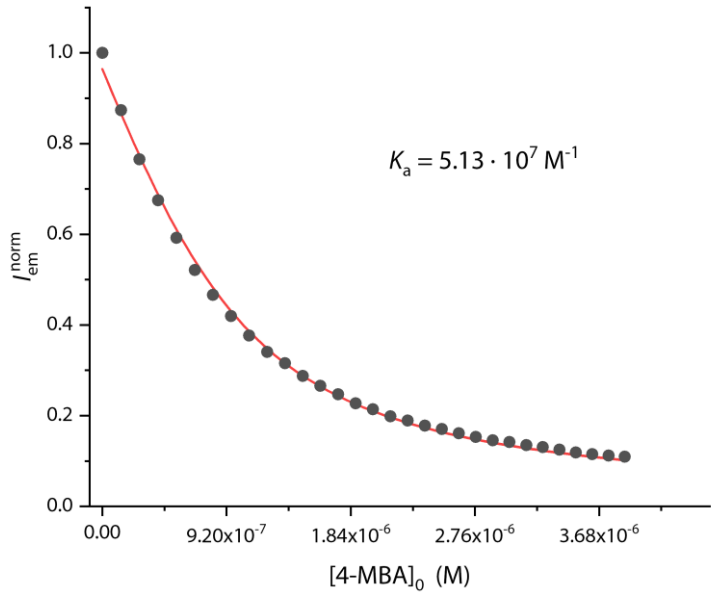

Fig. S3: Representative IDA binding isotherm determined by fluorescence intensity variations (λ_{exc} = 519 nm, λ_{em} = 575 nm) of DSMI (2.11 µM), CB6 (1.03 µM) and 4-MBA (0-3.87 µM) in water (3.87 µM HCl) at pH 7 at 25°C. Acquired data is depicted as gray dots and fitted data as red line.

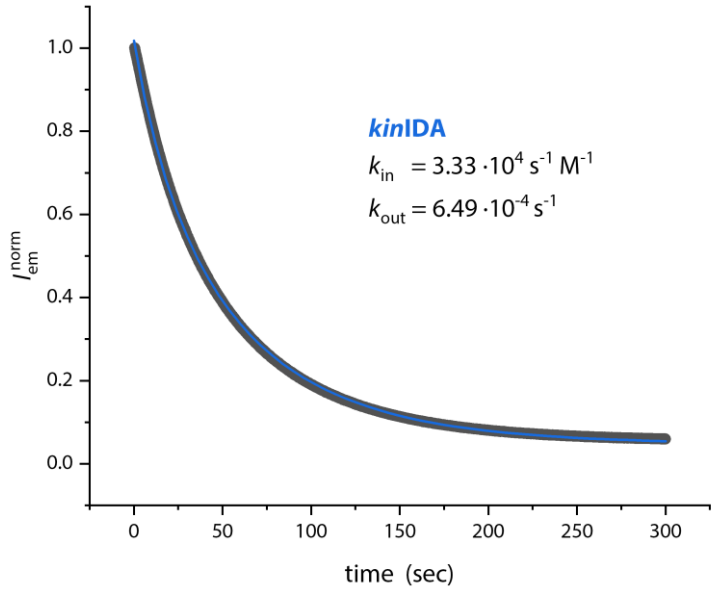

Fig. S4: Representative IDA kinetic binding curve determined by fluorescence intensity variations (λ_{exc} = 519 nm, λ_{em} = 575 nm) of DSMI (2.08 µM), CB6 (1.05 µM) and 4-MBA (8.23 µM) in water (8.23 µM HCl) at pH 7 at 25°C. Acquired data are depicted as gray dots and fitted data following the competitive binding model (Eq. S14) as blue line.

4.3.3 CB7⊃BE

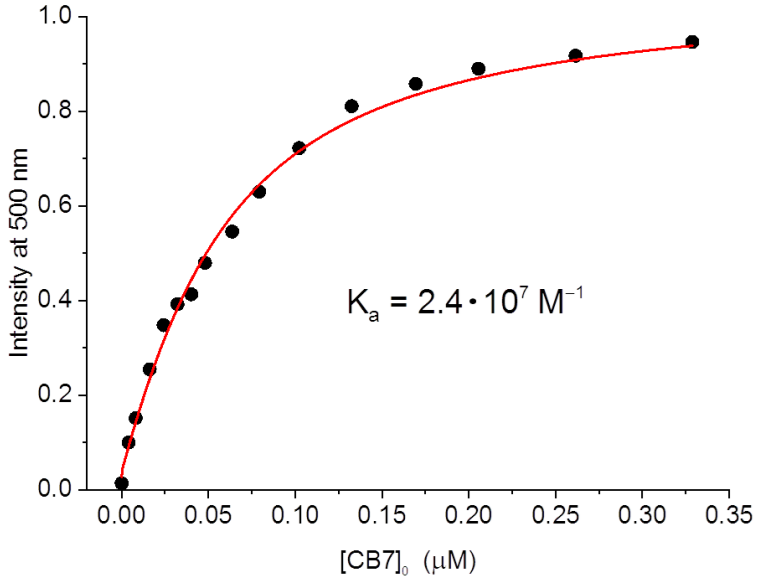

Fig. S5: Representative DBA binding isotherm at 25°C determined by fluorescence titration (λ_{exc} = 345 nm, λ_{em} = 500 nm) of chromatographically purified BE (0.034 µM) with CB7 (0 – 0.35 µM) in water freshly distilled three times from dilute $KMnO_4$ solution. Acquired data are depicted as gray dots and fitted data as red line.

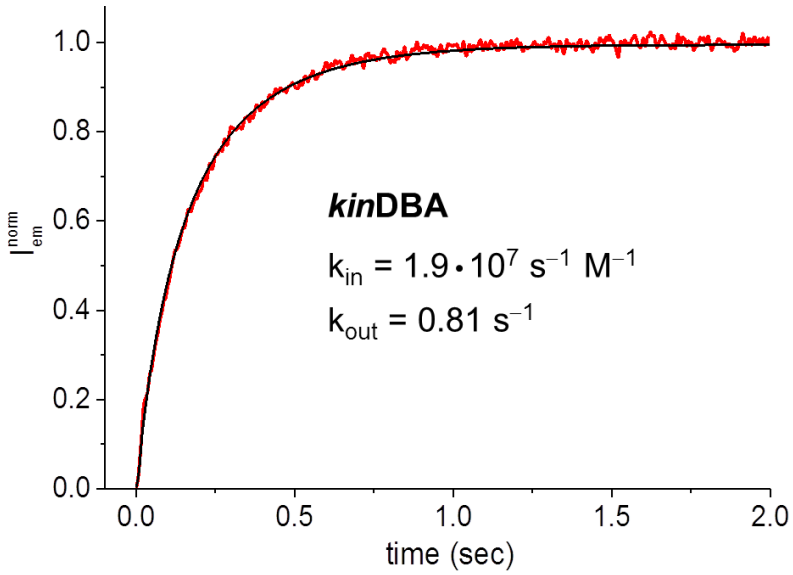

Fig. S6: Representative DBA kinetic binding curve at 25°C determined by fluorescence intensity variations (λ_{exc} = 345 nm, λ_{em} = 500 nm) of chromatographically purified BE (0.23 µM) with CB7 (0.23 µM) in water freshly distilled three times from dilute $KMnO_4$ solution. Acquired data are depicted as red line and fitted data as black line.

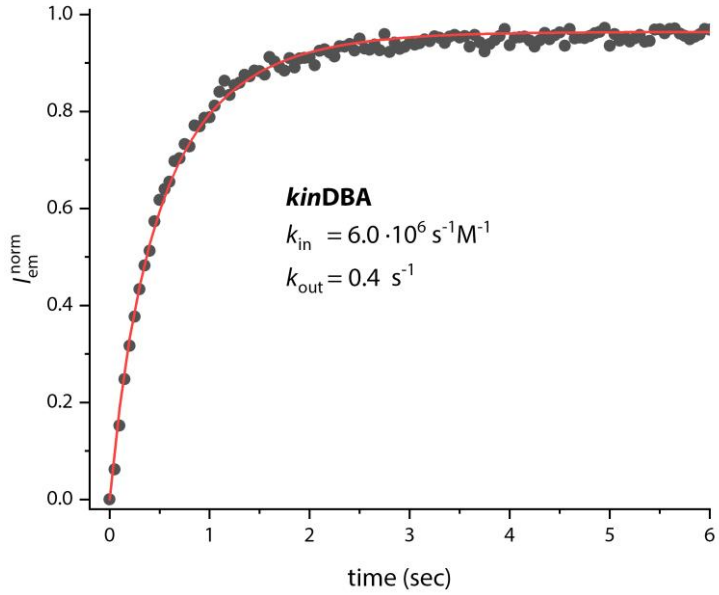

Fig. S7: Representative DBA kinetic binding curve determined by fluorescence intensity variations (λ_{exc} = 465 nm, λ_{em} = 525 nm) of BE (0.2 µM) and CB7 (0.3 µM) in water at 25°C. Acquired data are depicted as gray dots and fitted data as red line.

4.3.4 CB7⊃MDAP

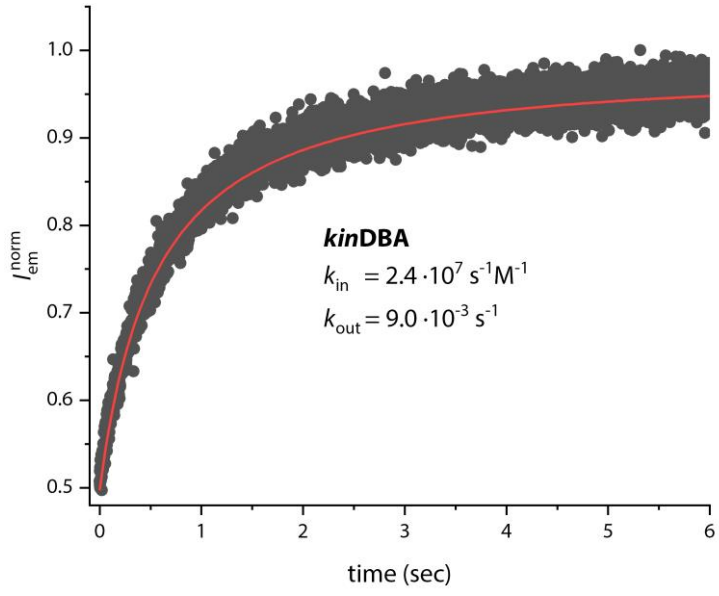

Fig. S8: Representative DBA kinetic binding curve determined by fluorescence intensity variations (λ_{exc} = 339 nm, λ_{em} = 454 nm) of MDAP (71 nM), and CB7 (72 nM) in water at 25°C. Acquired data are depicted as gray dots and fitted data as red line.

4.3.5 CB7⊃nandrolone

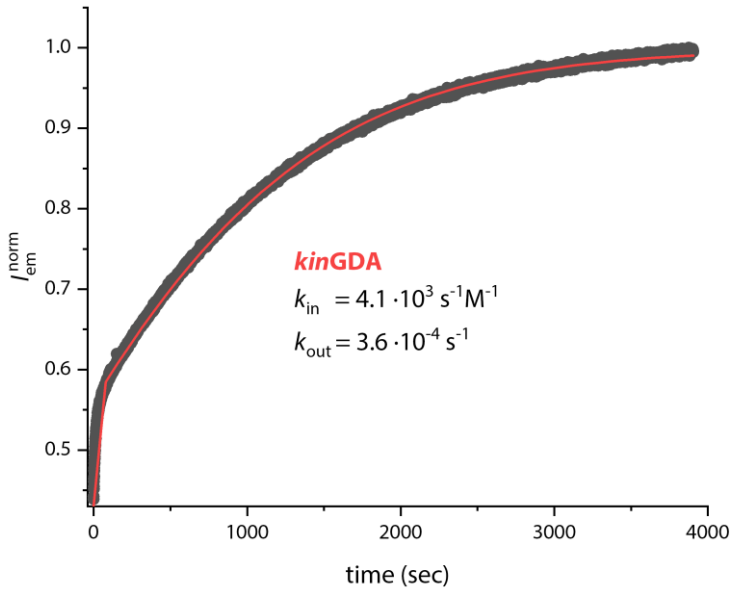

Fig. S9: Representative GDA kinetic binding curve determined by fluorescence intensity variations (λ_{exc} = 462 nm, λ_{em} = 540 nm) of BE (2 µM), nandrolone (2 µM) and CB7 (2 µM) in water at 25°C. Acquired data are depicted as gray dots and fitted data following the competitive binding model (Eq. S14) as red line.

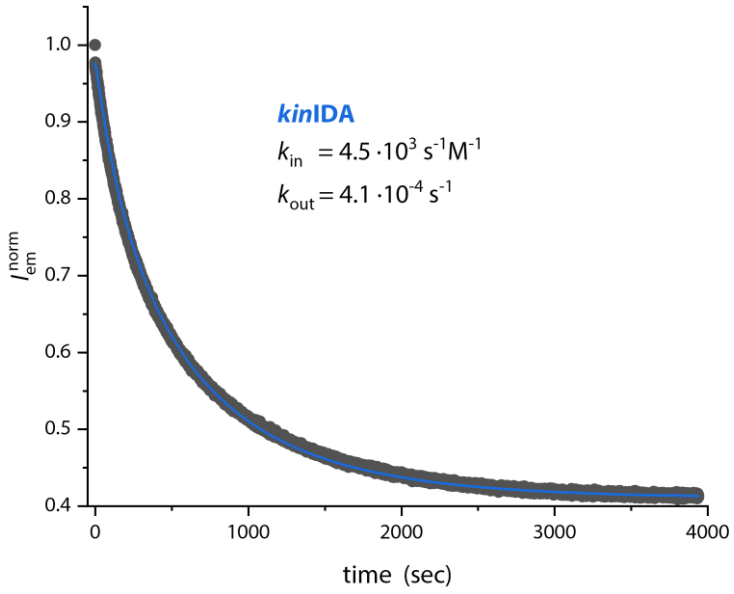

Fig. S10: IDA kinetic binding curve determined by fluorescence intensity variations (λ_{exc} = 462 nm, λ_{em} = 540 nm) of BE (2 µM), nandrolone (2 µM) and CB7 (2 µM) in water at 25°C. Acquired data are depicted as gray dots and fitted data following the competitive binding model (Eq. S14) as blue line.

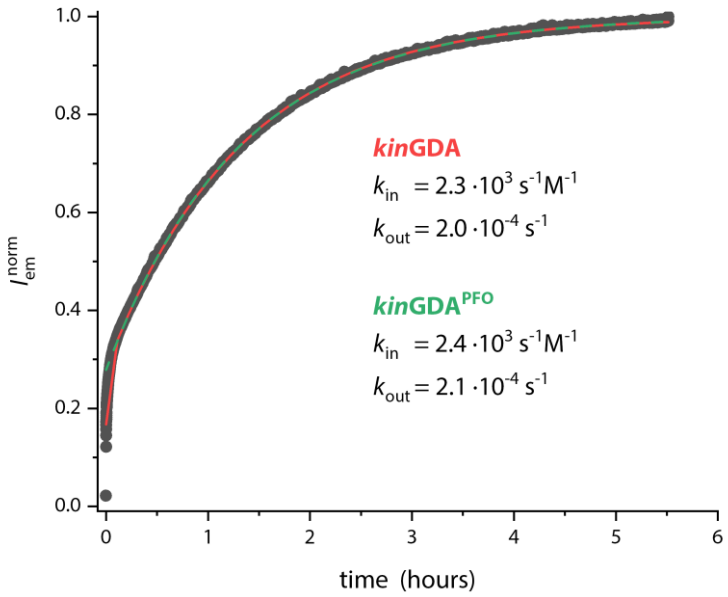

Fig. S11: Representative GDA kinetic binding curve determined by fluorescence intensity variations (λ_{exc} = 462 nm, λ_{em} = 540 nm) of BE (50 µM), nandrolone (2 µM) and CB7 (2 µM) in water at 25°C. Acquired data are depicted as gray dots and fitted data following the competitive binding model (Eq. S14) as red line and following the pseudo-first order model (Eq. S22) as green line.

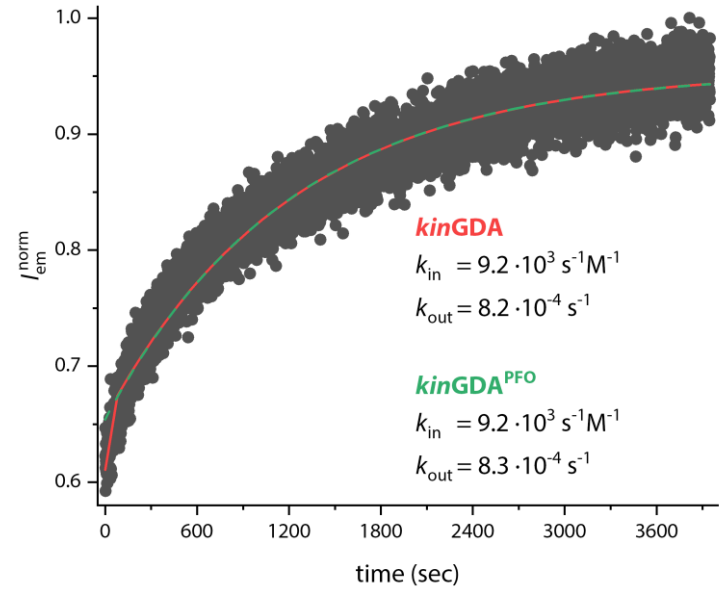

Fig. S12: Representative GDA kinetic binding curve determined by fluorescence intensity variations (λ_{exc} = 343 nm, λ_{em} = 454 nm) of MDAP (40 µM), nandrolone (2 µM) and CB7 (2 µM) in water at 25°C. Acquired data are depicted as gray dots and fitted data following the competitive binding model (Eq. S14) as red line and following the pseudo-first order model (Eq. S22) as green line.

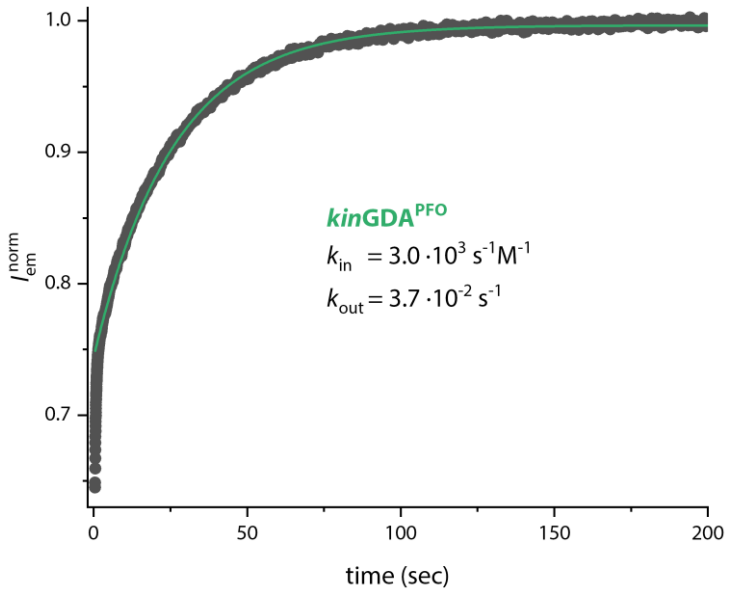

Fig. S13: Representative GDA kinetic binding curve determined by fluorescence intensity variations (λ_{exc} = 462 nm, λ_{em} = 550 nm) of BE (50 µM), nandrolone (2 µM) and CB7 (2 µM) in in sodium phosphate buffer (50 mM) at 25°C. Acquired data are depicted as gray dots and fitted data following the pseudo-first order model (Eq. S22) as green line.

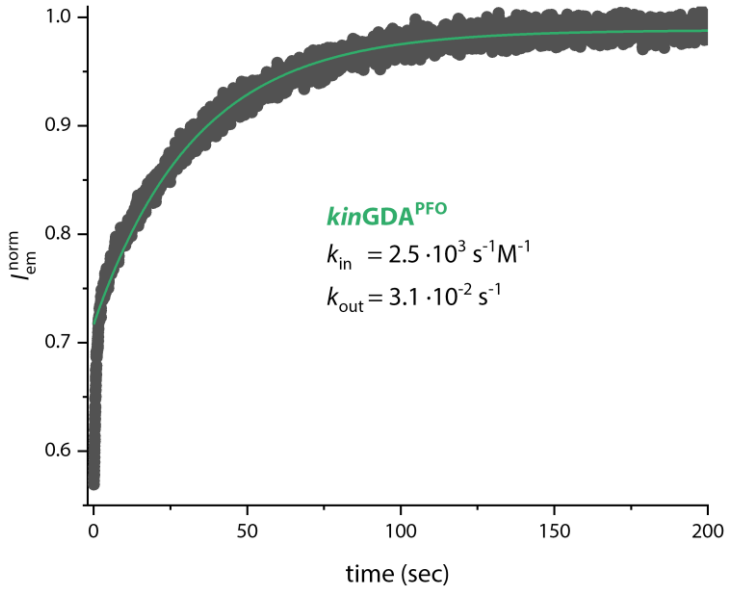

Fig. S14: Representative GDA kinetic binding curve determined by fluorescence intensity variations (λ_{exc} = 343 nm, λ_{em} = 454 nm) of MDAP (25 µM), nandrolone (2 µM) and CB7 (2 µM) in sodium phosphate buffer (50 mM) at 25°C. Acquired data are depicted as gray dots and fitted data following the pseudo-first order model (Eq. S22) as green line.

4.3.6 CB7⊃cholesterol

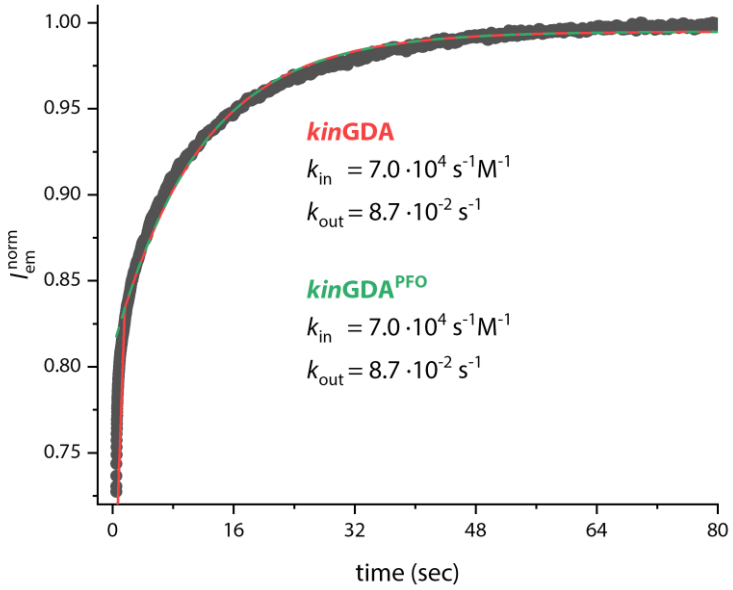

Fig. S15: Representative GDA kinetic binding curve determined by fluorescence intensity variations (λ_{exc} = 462 nm, λ_{em} = 550 nm) of BE (50 µM), cholesterol (2.45 µM) and CB7 (2.22 µM) in water/ethanol (99.9/0.1, v/v) mixture at 25°C. Acquired data are depicted as gray dots and fitted data following the competitive binding model (Eq. S14) as red line and following the pseudo-first order model (Eq. S22) as green line.

4.3.7 CB7⊃estradiol

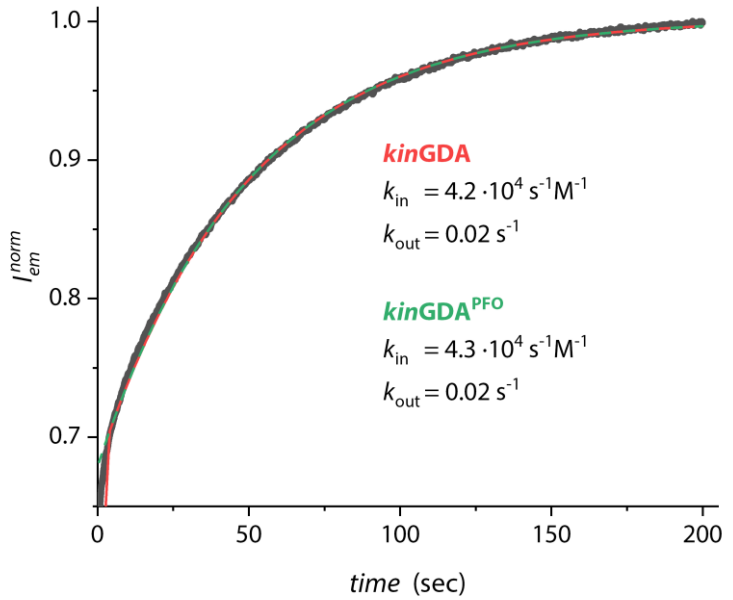

Fig. S16: Representative GDA kinetic binding curve determined by fluorescence intensity variations (λ_{exc} = 462 nm, λ_{em} = 550 nm) of BE (50 µM), estradiol (3.9 µM) and CB7 (3.9 µM) in water at 25°C. Acquired data are depicted as gray dots and fitted data following the competitive binding model (Eq. S14) as red line and following the pseudo-first order model (Eq. S22) as green line.

4.3.8 CB7(desalted)⊃BE

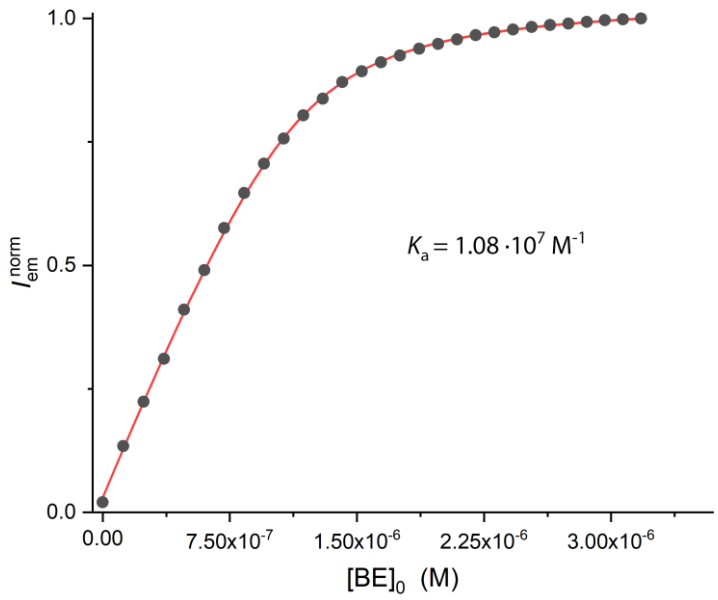

Figure S17: Representative DBA binding isotherm determined by fluorescence intensity variations (λ_{exc} = 440 nm, λ_{em} = 542 nm) of desalted CB7 (1.15 µM) and BE (0-3.2 µM) in water at 25°C. Acquired data are depicted as gray dots and fitted data as red line.

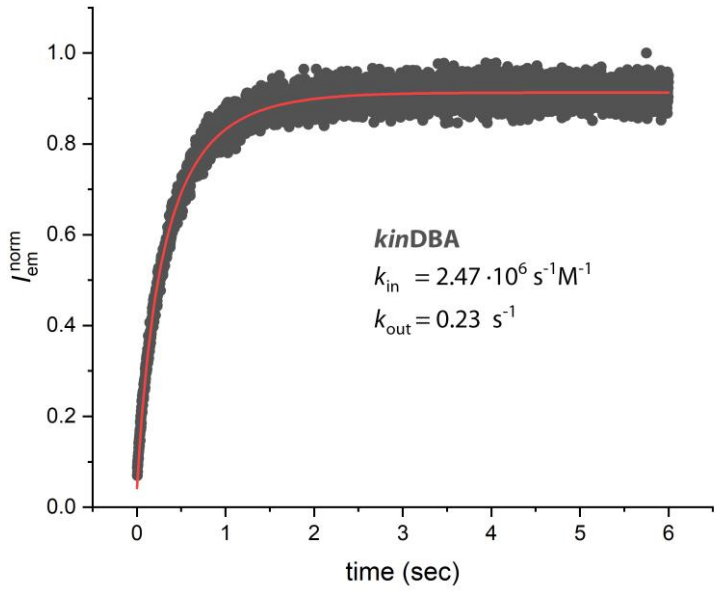

Figure S18: Representative DBA kinetic binding curve determined by fluorescence intensity variations (λ_{exc} = 430 nm, λ_{em} = 530 nm) of BE (1.2 µM) and desalted CB7 (1 µM) in water at 25°C. Acquired data are depicted as gray dots and fitted data as red line.

4.3.9 CB7(desalted)⊃adamantanol

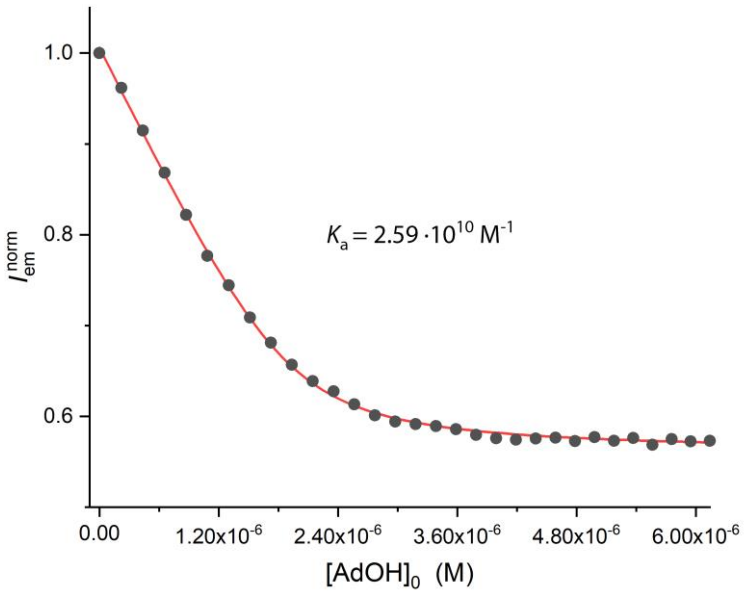

Figure S19: Representative IDA binding isotherm determined by fluorescence intensity variations (λ_{exc} = 378 nm, λ_{em} = 427.5 nm) of MDAP (3.0 µM), desalted CB7 (2.0 µM) and AdOH (0-6 µM) in water at 25°C. Acquired data are depicted as gray dots and fitted data as red line.

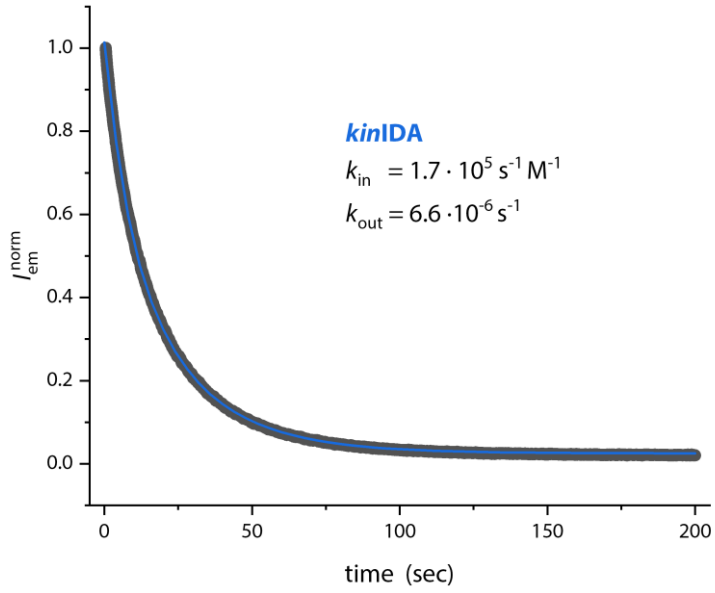

Fig. S20: Representative IDA binding curve determined by fluorescence intensity (λ_{exc} = 430 nm and λ_{em} = 530 nm) of BE (1.2 µM), CB7 (1 µM) and adamantanol (5 µM) in water at 25°C. Acquired data are depicted as gray dots and fitted data following the competitive binding model (Eq. S14) as blue line.

4.3.10 CB7⊃(+)-fenchone

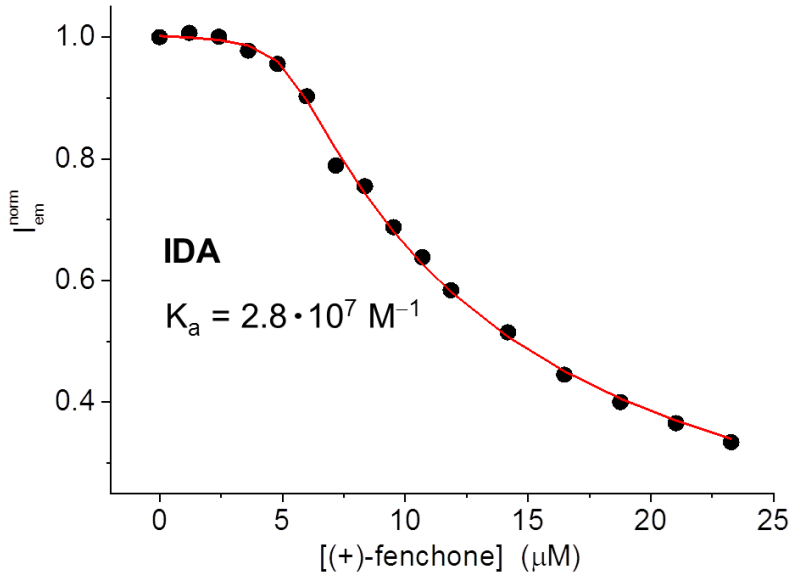

Fig. S21: Representative IDA binding curve determined at 25°C by fluorescence intensity variations (λ_{exc} = 345 nm, λ_{em} = 503 nm) of chromatographically purified BE (5.0 µM), (+)-fenchone (0 - 23 µM) and CB7 (10.2 µM) in water freshly distilled three times from dilute $KMnO_4$ solution. Acquired data are depicted as black dots and fitted data as red line.

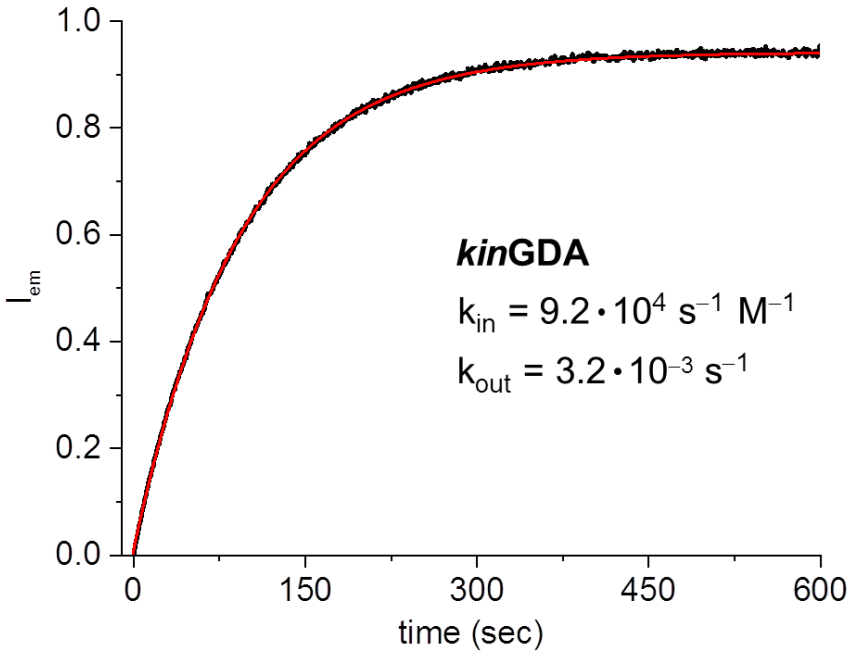

Fig. S22: Representative GDA kinetic binding curve determined at 25°C by fluorescence intensity variations (λ_{exc} = 345 nm, λ_{em} = 505 nm) of chromatographically purified BE (2.5 µM), (+)-fenchone (5.1 µM) and CB7 (0.25 µM) in water freshly distilled three times from dilute $KMnO_4$ solution. Acquired data are depicted as black line and fitted data following the competitive binding model (Eq. S14) as red line.

4.3.11 CB7⊃norcamphor

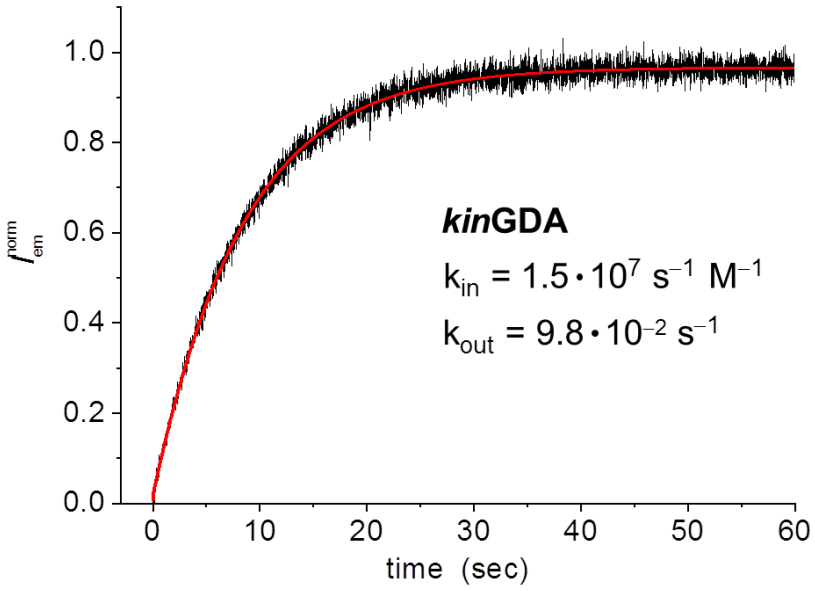

Fig. S23: Representative GDA kinetic binding curve determined at 25°C by fluorescence intensity variations (λ_{exc} = 422 nm, λ_{em} = 510 nm) of chromatographically purified BE (32 µM), norcamphor (0.35 µM) and CB7 (0.25 µM) in water freshly distilled three times from dilute $KMnO_4$ solution. Acquired data are depicted as black line and fitted data following the competitive binding model (Eq. S14) as red line.

4.3.12 CB8⊃MPCP

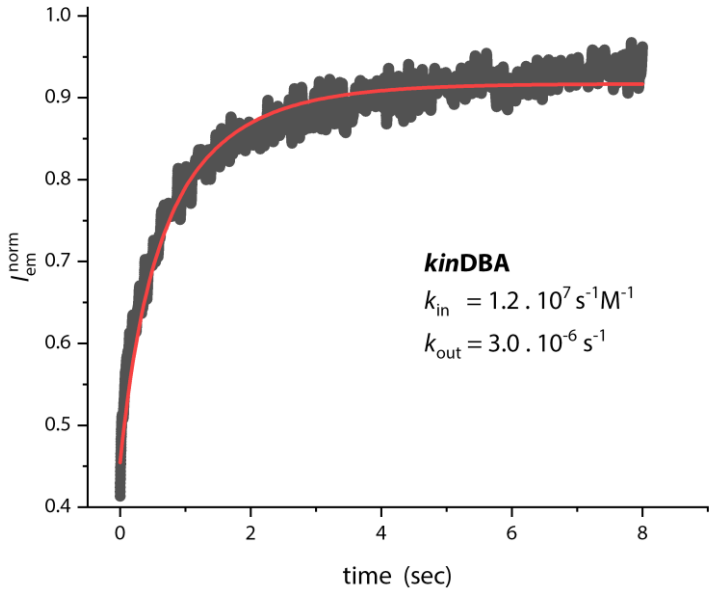

Fig. S24: Representative DBA kinetic binding curve determined by fluorescence intensity variations (λ_{exc} = 366 nm, λ_{em} = 533 nm) of MPCP (0.2 µM) and CB8 (0.1 µM) in water at 25°C. Acquired data are depicted as gray dots and fitted data as red line. Note: Data was smoothed before fitting (25 points Savitzky-Golay).

4.3.13 CB8⊃nandrolone

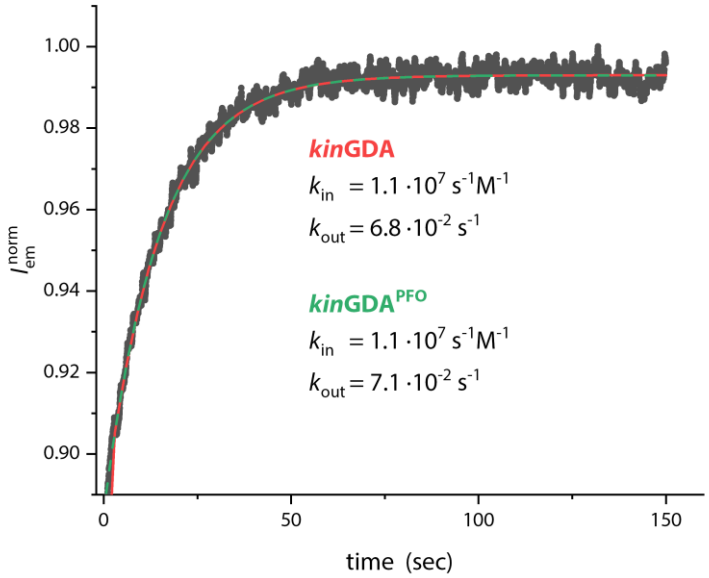

Fig. S25: Representative GDA kinetic binding curve determined by fluorescence intensity variations (λ_{exc} = 366 nm, λ_{em} = 533 nm) of MPCP (50 µM), nandrolone (1 µM) and CB8 (1 µM) in water at 25°C. Acquired data are depicted as gray dots and fitted data following the competitive binding model (Eq. S14) as red line and following the pseudo-first order model (Eq. S22) as green line.

4.3.14 CB8⊃testosterone

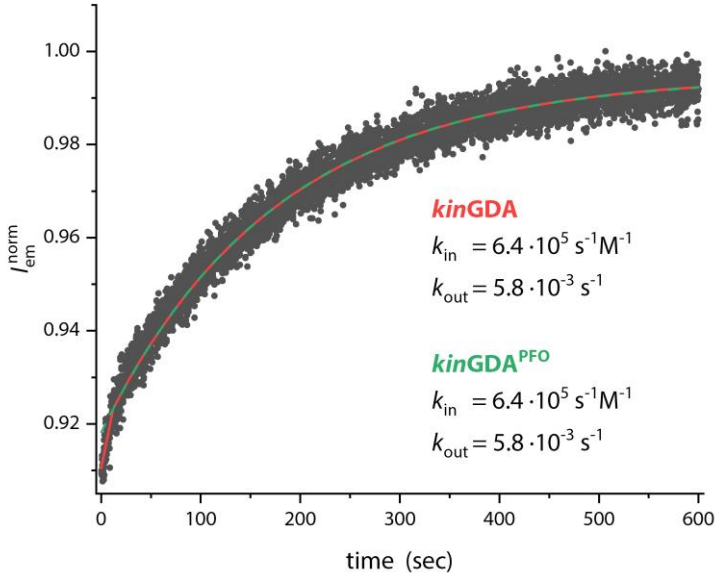

Fig. S26: Representative GDA kinetic binding curve determined by fluorescence intensity variations (λ_{exc} = 366 nm, λ_{em} = 533 nm) of MPCP (50 µM), testosterone (5 µM) and CB8 (5 µM) in water at 25°C. Acquired data are depicted as gray dots and fitted data following the competitive binding model (Eq. S14) as red line and following the pseudo-first order model (Eq. S22) as green line.

4.3.15 CB8⊃prednisolone

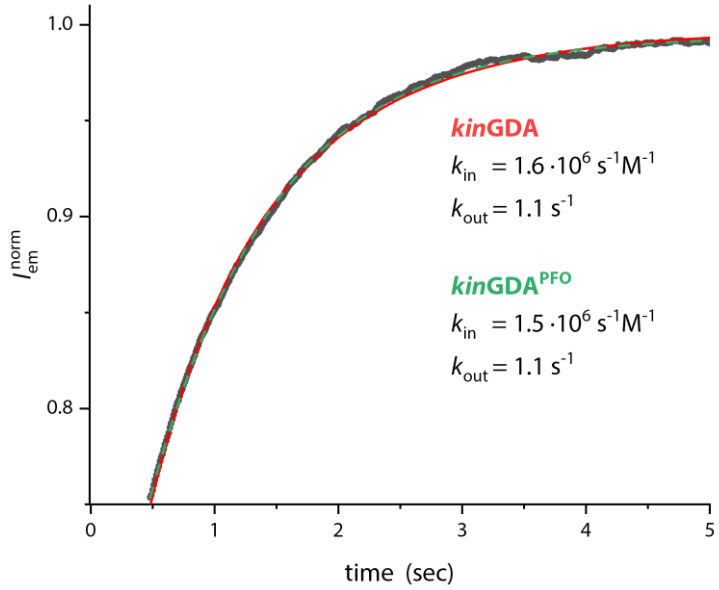

Fig. S27: Representative GDA kinetic binding curve determined by fluorescence intensity variations (λ_{exc} = 366 nm, λ_{em} = 533 nm) of MPCP (50 µM), prednisolone (5 µM) and CB8 (5 µM) in water at 25°C. Acquired data are depicted as gray dots and fitted data following the competitive binding model (Eq. S14) as red line and following the pseudo-first order model (Eq. S22) as green line.

4.3.16 CB8(desalted)⊃MPCP

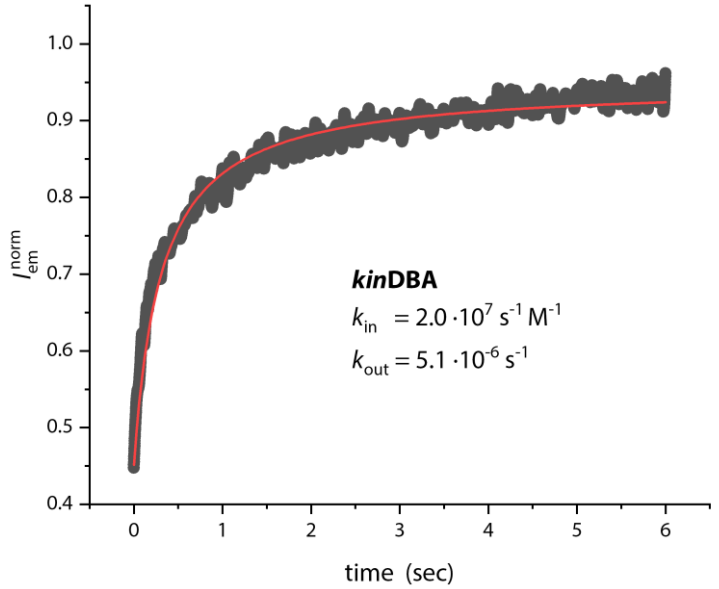

Fig. S28: Representative DBA kinetic binding curve determined by fluorescence intensity variations (λ_{exc} = 366 nm, λ_{em} = 533 nm) of MPCP (0.2 µM) and desalted CB8 (0.21 µM) in water at 25°C. Acquired data are depicted as gray dots and fitted data as red line. Note: Data was smoothed before fitting (25 points Savitzky-Golay).

4.3.17 CB8(desalted)⊃adamantanol

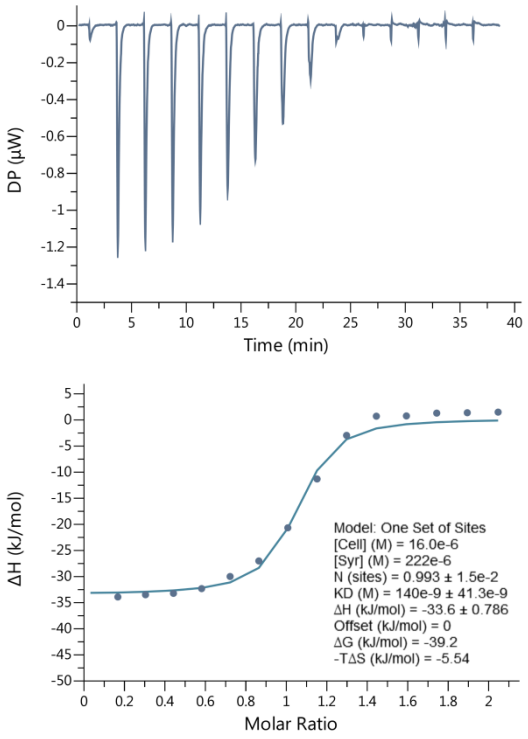

Fig. S29: Representative ITC isotherms of desalted CB8 (16 µM) and 1-adamantanol (0 – 40 µM) in water at 25°C.

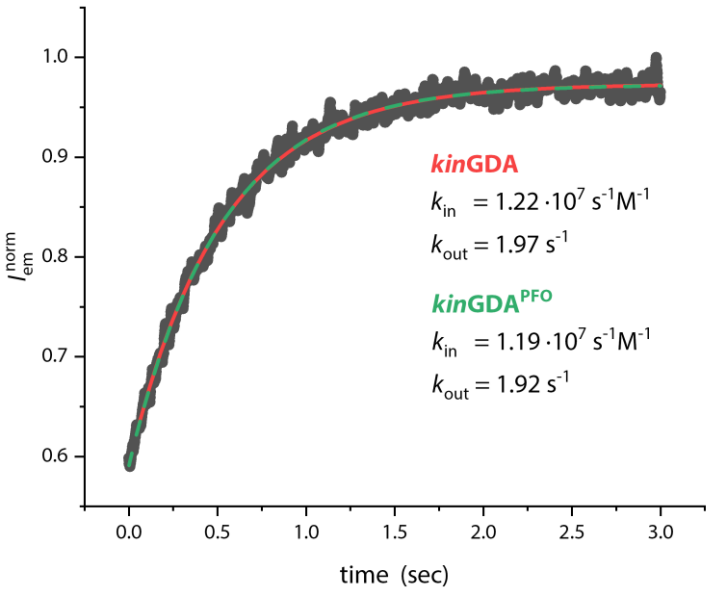

Fig. S30: Representative GDA kinetic binding curve determined by fluorescence intensity variations (λ_{exc} = 366 nm, λ_{em} = 533 nm) of MPCP (10 µM), adamantanol (1.43 µM) and desalted CB8 (1 µM) in water at 25°C. Acquired data are depicted as gray dots and fitted data following the competitive binding model (Eq. S14) as red line and following the pseudo-first order model (Eq. S22) as green line. Note: Data was smoothed before fitting (25 points Savitzky-Golay).

4.3.18 CB8(desalted)⊃ferrocenyl methanol

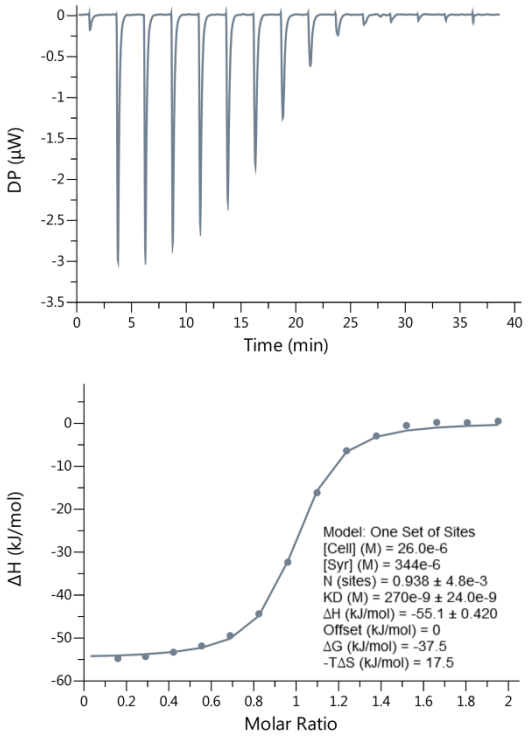

Fig. S31: Representative ITC isotherms of desalted CB8 (26 µM) and ferrocenyl methanol (0 – 60 µM) in water at 25°C.

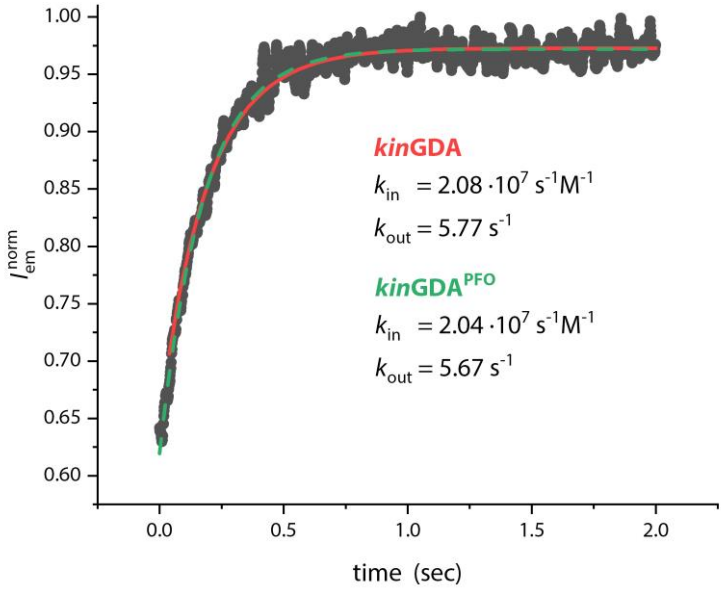

Fig. S32: Representative GDA kinetic binding curve determined by fluorescence intensity variations (λ_{exc} = 366 nm, λ_{em} = 533 nm) of MPCP (5.25 µM), ferrocenyl methanol (0.8 µM) and desalted CB8 (0.56 µM) in water at 25°C. Acquired data are depicted as gray dots and fitted data following the competitive binding model (Eq. S14) as red line and following the pseudo-first order model (Eq. S22) as green line. Note: Data was smoothed before fitting (25 points Savitzky-Golay).

4.3.19 HSA⊃warfarin

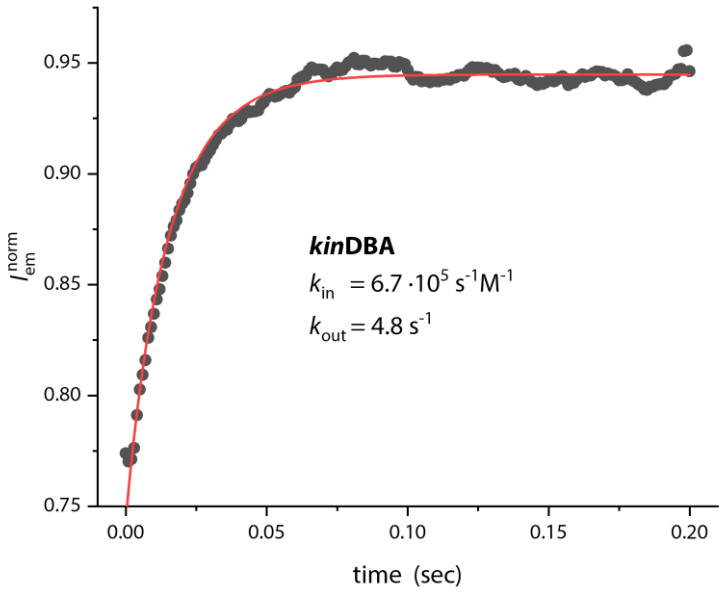

Fig. S33: Representative DBA kinetic binding curve determined by fluorescence intensity variations (λ_{exc} = 335 nm, λ_{em} = 410 nm) of warfarin (100 µM) and HSA (20 µM) in PBS at 25°C. Acquired data are depicted as gray dots and fitted data as red line. Note: Experimental data was smoothed for depiction (20 points adjacent averaging).

4.3.20 HSA⊃phenylbutazone

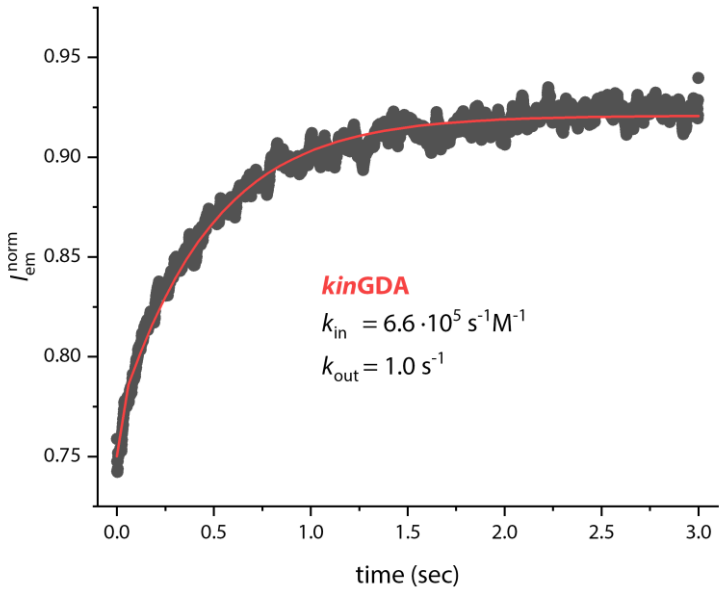

Fig. S34: Representative GDA kinetic binding curve determined by fluorescence intensity variations (λ_{exc} = 335 nm, λ_{em} = 410 nm) of warfarin (100 µM), PBZ (40 µM) and HSA (20 µM) in PBS at 25°C. Acquired data are depicted as gray dots and fitted data following the competitive binding model (Eq. S14) as red line. Note: Experimental data was smoothed for depiction (20 points adjacent averaging).

5 Kinetic and Thermodynamic Correlation Analysis

5.1 Van't Hoff and Eyring Equations

$$\Delta G = -RT \cdot \ln K_a \qquad \text{Eq. S23}$$

$$\Delta G_{in}^{\#} = -RT \cdot \ln\left(\frac{k_{in}}{k_B T/h}\right) \qquad \text{Eq. S24}$$

$$\Delta G_{out}^{\#} = -RT \cdot \ln\left(\frac{k_{out}}{k_B T/h}\right) \qquad \text{Eq. S25}$$

R – universal gas constant (8.3145 J K^{-1} mol^{-1}),
k_B – Boltzmann constant ($1.381 \cdot 10^{-23}$ J K^{-1}),
T – temperature (in K),
h – Planck constant ($6.63 \cdot 10^{-34}$ J s),
K_a – binding constant,
ΔG – Gibbs free energy for the formation (association) of the complex,
k_{in} – kinetic rate constant for the association of the complex (complexation),
$\Delta G_{in}^{\#}$ – Gibbs energy of activation for the association of the complex,
k_{out} – kinetic rate constant for the dissociation of the complex (decomplexation),
$\Delta G_{out}^{\#}$ – Gibbs energy of activation for the dissociation of the complex,
Note: This approach assumes a conversion towards the products from a single transition state (either for association or for dissociation) and thus the transmission coefficient κ is taken to be unity.[16]
Representative CB6 complexes that were slow enough to be determined by NMR binding studies (*kin*DBA), were obtained in solvent mixtures or buffers due to solubility limitations.[17, 18]

5.2 Correlation Data

Table S4: Data used for correlation analysis in Figure 4 (main text). If not stated differently, values are acquired in this work by fluorescence titration and listed in Table S3.

host	guest	T / °C	log (K_a / M^{-1})	k_{in} / M^{-1} s^{-1}	k_{out} / s^{-1}	ΔG / kJ mol^{-1}	$\Delta G^{\#}_{in}$ / kJ mol^{-1}	$\Delta G^{\#}_{out}$ / kJ mol^{-1}
CB6	DSMI	25	6.90	$2.0 \cdot 10^8$	$2.44 \cdot 10^1$	-39.4	25.7	65.1
CB6	4-MBA [a]	25	7.71	$3.3 \cdot 10^4$	$6.49\ 10^{-4}$	-44.0	47.2	91.2
CB6	cyclobutylmethylamine [17]	40	5.57	$5.9 \cdot 10^3$	$1.6 \cdot 10^{-2}$	-33.4	54.2	87.6
CB6	cyclopentylmethylamine [17]	40	5.52	5.5	$1.6 \cdot 10^{-5}$	-33.1	72.4	105.6
CB6	cyclohexylmethylamine [17]	40	1.90	$8.8 \cdot 10^{-4}$	$1.1 \cdot 10^{-5}$	-11.4	95.1	106.6
CB6	4-MBA [b] [18]	40	2.51	2.7	$8.5 \cdot 10^{-3}$	-15.0	74.2	89.2
CB6	cyclohexylmethylamine Na^+ [18]	25	1.67	$2.4 \cdot 10^{-4}$	$5.1 \cdot 10^{-6}$	-9.5	93.7	103.2
CB6	cyclohexylmethylamine K^+ [18]	25	1.83	$2.6 \cdot 10^{-4}$	$3.9 \cdot 10^{-6}$	-10.4	93.5	103.9
CB6	cyclohexylmethylamine Rb^+ [18]	25	1.92	$3.2 \cdot 10^{-4}$	$3.8 \cdot 10^{-6}$	-11.0	93.0	104.0
CB6	cyclohexylmethylamine Cs^+ [18]	25	1.95	$4.5 \cdot 10^{-4}$	$5.0 \cdot 10^{-6}$	-11.2	92.1	103.3
CB6	1,4-diaminocyclohexane [19]	25	6.15	$1.2 \cdot 10^{-3}$	$8.5 \cdot 10^{-10}$	-35.1	89.7	124.8
CB6	N-butyladamantan-1-aminium [19]	25	7.30	$4.4\ 10^4$	$2.2 \cdot 10^{-3}$	-41.7	46.5	88.2
CB7	nandrolone	25	7.05	$4.1\ 10^3$	$3.6 \cdot 10^{-4}$	-40.2	52.4	92.7
CB7	estradiol	25	6.25	$4.2\ 10^4$	$2.0 \cdot 10^{-2}$	-36.1	46.6	82.7
CB7	BE	25	7.23	$6.0 \cdot 10^6$	$3.5 \cdot 10^{-1}$	-41.3	34.4	75.6
CB7	cholesterol	25	5.91	$7.0\ 10^4$	$8.7 \cdot 10^{-2}$	-33.7	45.4	79.1
CB7	MDAP	25	9.43	$2.4\ 10^7$	$9.0 \cdot 10^{-3}$	-53.8	30.9	84.7
CB7	(+)-fenchone	25	7.46	$3.2\ 10^4$	$3.2 \cdot 10^{-3}$	-42.6	44.7	87.3
CB7	norcamphor	25	8.18	$1.5\ 10^7$	$9.8 \cdot 10^{-2}$	-46.7	32.1	78.8
CB7	Flavopereirine perchlorate [20]	25	7.79	$9.0\ 10^7$	1.6	-44.4	27.6	71.9
CB7	BE [12]	10	7.72	$8.8 \cdot 10^6$	$1.6 \cdot 10^{-1}$	-41.9	31.6	73.5
CB7	BE [12]	25	7.37	$1.9\ 10^7$	$8.1 \cdot 10^{-1}$	-42.1	31.5	73.5
CB7	((trimethylamino)methyl) ferrocene [21]	25	11.52	$2.0\ 10^7$	$7.0 \cdot 10^{-5}$	-65.8	31.3	96.7
CB7	R-(+)-2-naphthyl-1-ethylammonium cation [22]	25	7.03	$6.3\ 10^8$	$5.5 \cdot 10^1$	-40.1	22.8	63.1
CB7	N-butyladamantan-1-aminium [19]	25	12.00	$2.4\ 10^7$	$2.4 \cdot 10^{-5}$	-68.5	30.9	99.4
CB7	1,4-diaminocyclohexane [19]	25	8.36	$6.0 \cdot 10^8$	2.7	-47.7	22.9	70.6
CB7	6-methoxy-1-methylquinolinium[23]	24	6.30	$3.0 \cdot 10^9$	$1.5 \cdot 10^3$	-35.8	18.9	54.7
CB7	bis(3,5-dimethoxybenzyl)-4,4′-bipyridinium [24]	25	>3.53	$3.0 \cdot 10^{-1}$	$8.0 \cdot 10^{-5}$	<-20.2	76.0	96.4
CB7	bis(3,5-diethoxybenzyl)-4,4′-bipyridinium [24]	25	>5.9	$9.0 \cdot 10^{-1}$	$1.0 \cdot 10^{-6}$	< -33.7	73.3	107.3
CB7	3′,4′,7-trimethoxyflavylium ion [25]	20	6.19	$7.7 \cdot 10^7$	$5.0 \cdot 10^1$	-34.7	27.5	62.2
CB7	2-aminoanthracenium cation [26]	20	6.36	$2.3 \cdot 10^7$	$1.0 \cdot 10^1$	-35.7	30.4	66.1
CB7	1-tri(ethylene glycol)-1'-methyl-m-xylyl-4,4'-bipyridinium [27]	25	5.06	$6.0 \cdot 10^6$	$5.3 \cdot 10^1$	-28.9	34.3	63.2
CB7	1,1'-(1,4-phenylenebis(methylene)) bis(pyridin-1-ium-4-carboxylate [28]	25	5.81	$6.2 \cdot 10^{-1}$	$9.6 \cdot 10^{-7}$	-33.2	74.2	107.4
CB7	1,1'-(1,4-phenylenebis(methylene)) bis(pyridin-1-ium-3-carboxylate [28]	25	5.75	3.4	$6.0 \cdot 10^{-6}$	-32.8	70.0	102.8
CB7	N-phenyl-2-naphthyl ammonium cation [29]	20	5.48	$1.2 \cdot 10^7$	$3.87 \cdot 10^1$	-30.7	32.1	62.8
CB7	1,1'-bis(5-carboxypentyl)-[4,4'-bipyridine]-1,1'-diium [30]	20	5.57	$7.5\ 10^3$	$2.0 \cdot 10^{-2}$	-31.3	50.0	81.3

CB7(desalted)	BE	25	7.03	$2.5\ 10^6$	$2.3 \cdot 10^{-1}$	-40.1	36.5	76.7
CB7(desalted)	AdOH	25	10.41	$1.7 \cdot 10^5$	$6.6 \cdot 10^{-6}$	-59.4	43.2	102.6
CB8	testosterone	25	8.04	$6.4 \cdot 10^5$	$5.8 \cdot 10^{-3}$	-45.9	39.9	85.8
CB8	nandrolone	25	8.19	$1.1\ 10^7$	$7.1 \cdot 10^{-2}$	-46.8	32.8	79.6
CB8	prednisolone	25	6.15	$1.6\ 10^6$	1.1	-35.1	37.7	72.8
CB8	MPCP	25	12.59	$1.2\ 10^7$	$3 \cdot 10^{-6}$	-71.9	32.6	104.5
CB8	BE[31]	10	7.23	$6.4\ 10^7$	3.8	-39.2	26.9	66.1
CB8(desalted)	MPCP	25	12.59	$2.0 \cdot 10^7$	$5.1 \cdot 10^{-6}$	-71.9	31.3	103.2
CB8(desalted)	$FeCp_2OH$	25	6.56	$2.1 \cdot 10^7$	5.8	-37.5	31.3	68.7
CB8(desalted)	AdOH	25	6.79	$1.2 \cdot 10^7$	1.97	-38.8	32.6	71.3
CB8⊃BE	BE[31]	10	6.92	$5.0 \cdot 10^6$	$6.0 \cdot 10^{-1}$	-37.5	32.9	70.4
CB8⊃MV	1-Naphthylamine-PEG [32]	5	4.60	$2.5\ 10^7$	$3.9 \cdot 10^2$	-24.5	28.6	54.2
CB8⊃MV	2-Naphthylamine-PEG [32]	5	≥5.30	$4.0\ 10^7$	$\leq 2.0 \cdot 10^2$	≤-28.2	27.5	55.7
CB8⊃MV	Anthracene-PEG [32]	5	≥6.45	$2.8\ 10^7$	$\leq 1.0 \cdot 10^1$	≤-34.3	28.3	62.6
CB8⊃MV	Fluorene-PEG [32]	5	≥6.45	$2.8\ 10^7$	$\leq 1.0 \cdot 10^1$	≤-34.3	28.3	62.6
CB8⊃MV	Dibenzofuran-PEG [32]	5	5.83	$2.2\ 10^7$	$3.2 \cdot 10^1$	-31.1	28.9	59.9
CB8⊃MV	Pyrene-PEG [32]	5	6.36	$1.9\ 10^7$	8.0	-33.9	29.2	63.2
HSA	PBZ	25	5.83	$6.6\ 10^5$	$9.7 \cdot 10^{-1}$	-33.3	39.8	73.1
HSA	warfarin	25	5.15	$6.7\ 10^5$	4.8	-29.4	39.8	69.1
HSA	tolbutamide [33]	37	5.04	$6.5\ 10^4$	$5.9 \cdot 10^{-1}$	-29.9	47.5	77.4
HSA	acetohexamide [33]	37	5.26	$1.2\ 10^5$	$6.7 \cdot 10^{-1}$	-31.2	45.9	77.1
HSA	verapamil [33]	37	4.18	$5.3\ 10^3$	$3.5 \cdot 10^{-1}$	-24.8	54.0	78.8
HSA	gliclazide [33]	37	4.90	$4.9\ 10^4$	$6.1 \cdot 10^{-1}$	-29.1	48.2	77.3
HSA	chlorpromazine [33]	37	4.79	$2.5\ 10^5$	3.96	-28.5	44.1	72.5

[a] measured in water by fluorescence based *kin*GDA [b] measured in D_2O : formic acid (1:1) mixture by NMR

6 Determination of Concentrations of Host-Guest Complexes by NMR

The concentration determination of all insoluble guest molecules where carried out via ^{1}H NMR measurements in D_2O with dimethyl sulfone as a common standard.

For the measurement, the host-guest stock solution was prepared in D_2O and sonicated for 10 min. Afterwards, 0.25 ml of the solution were mixed with 0.25 ml of a dimethyl sulfone stock solution of which the concentration was known. The NMR measurement was then carried out on a Bruker Avance 500 spectrometer.

The obtained spectra were phase and baseline corrected and then calibrated to the solvent peak of D_2O. The signal of dimethyl sulfone at 3.08 ppm was used as a reference with a total integral of 6 protons. The integration of certain host and guest signals lead to the determination of the concentration of each compound.

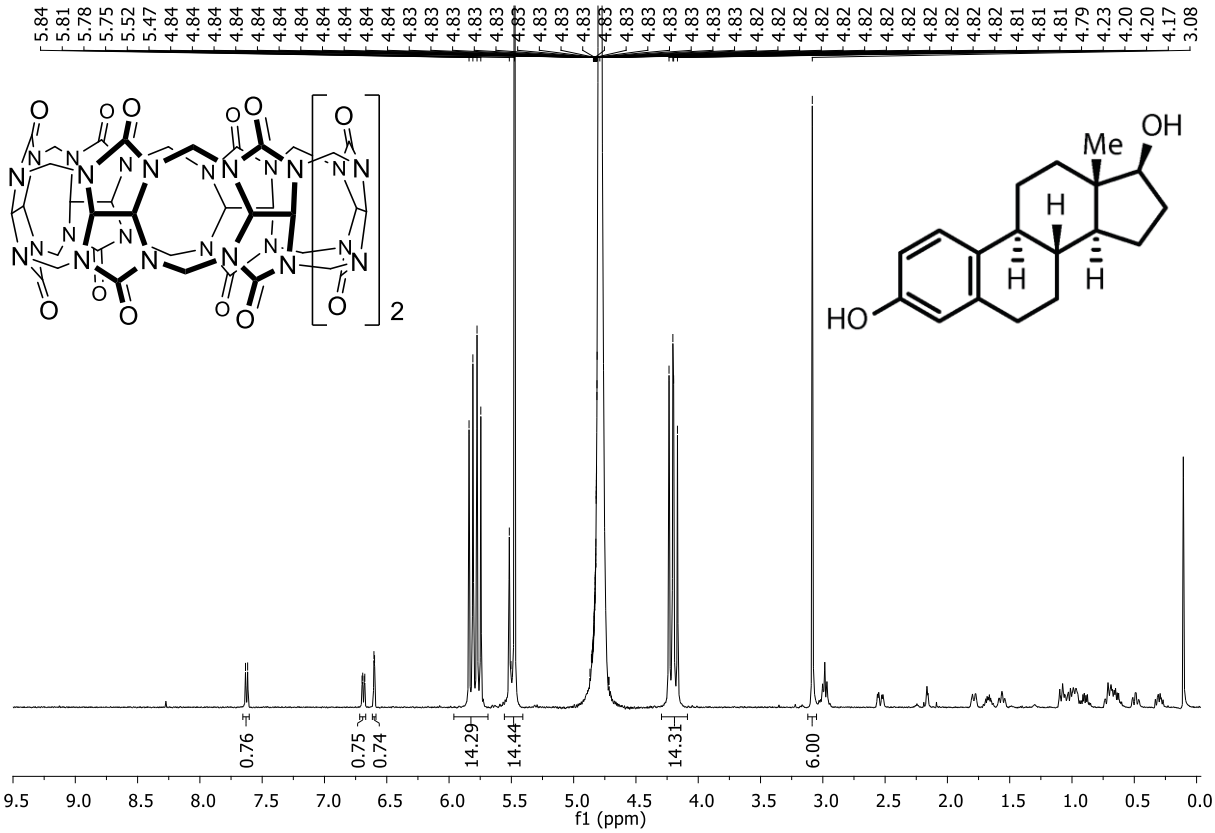

Fig. S5: ^{1}H NMR (500 MHz, D_2O) spectrum of the CB7/estradiol complex. All signals in the region of 0.20 to 2.60 ppm and 6.60 to 7.63 ppm can be referred to estradiol. For the concentration determination of estradiol only the signal from 6.60 to 7.63 ppm were integrated and used. The signals in the region 4.17 to 4.23 ppm and 5.47 to 5.84 ppm can be referred to CB7, they were all used for the concentration determination of CB7. The signal at 3.08 ppm can be referred to dimethyl sulfone, which was used as a proton reference for the concentration determination of all compounds.

Table S5: Calculation of the concentration of CB7 (top) and estradiol (bottom) *via* the received integrals from **Fig. S5**.

species	integral	protons	norm. integral	divisor	conc. [mM]
DMS	6.00	6.0	1.00000		1.00000
CB7-1	14.31	14.0	1.02214	0.97834	1.02214
CB7-2	14.44	14.0	1.03143	0.96953	1.03143
CB7-3	14.29	14.0	1.02071	0.97971	1.02071
CB7-Mean					1.02476
CB7-StDev					0.00582

species	integral	protons	norm. integral	divisor	conc. [mM]
DMS	6.00	6.00	1.00000		1.00000
estradiol	0.74	1.00	0.74000	1.35135	0.74000
estradiol	0.75	1.00	0.75000	1.35135	0.74000
estradiol	0.76	1.00	0.76000	1.31579	0.76000
estradiol-Mean					0.74667
estradiol-StDev					0.00943

7 References

1. B. Bendeby, L. Kenne and C. Sandström, *J. Incl. Phenom. Macrocycl. Chem.*, 2004, **50**, 173-181.
2. https://www.drugbank.ca/drugs/DB00812, PBZ, https://www.drugbank.ca/drugs/DB00812, (accessed 2019.12.02).
3. A. I. Lazar, F. Biedermann, K. R. Mustafina, K. I. Assaf, A. Hennig and W. M. Nau, *J. Am. Chem. Soc.*, 2016, **138**, 13022-13029.
4. M. J. Pilling, *Low-temperature combustion and autoignition*, Elsevier, 1997.
5. C. Wang, S. R. Perumalla, R. Lu, J. Fang and C. C. Sun, *Cryst. Growth Des.*, 2016, **16**, 933-939.
6. T. Janoschka, N. Martin, M. D. Hager and U. S. Schubert, *Angew. Chem. Int. Ed.*, 2016, **55**, 14427-14430.
7. *https://www.smellspedia.com/raw-material/d-fenchone/*.
8. A. S. Saratikov, L. A. Pchelkina, N. A. Belikova, A. A. Bobyleva, N. F. Dubitskaya, M. D. Ordubadi, S. K. Ermolaeva and A. F. Plate, *Pharm. Chem. J.*, 1977, **11**, 643-645.
9. S. R. J. Hoare, *J. Pharmacol. Toxicol. Methods*, 2018, **89**, 26-38.
10. H. J. Motulsky and L. C. Mahan, *Mol. Pharmacol.*, 1984, **25**, 1.
11. C. A. Schalley, *Analytical Methods in Supramolecular Chemistry*, Wiley, Weinheim, 2012.
12. Z. Miskolczy and L. Biczók, *J. Phys. Chem. B*, 2014, **118**, 2499-2505.
13. S. Sinn, J. Kraemer and F. Biedermann, *in press*, 2020.
14. S. Zhang, L. Grimm, Z. Miskolczy, L. Biczok, F. Biedermann and W. M. Nau, *Chem Commun (Camb)*, 2019, **55**, 14131-14134.
15. S. Sinn, E. Spuling, S. Bräse and F. Biedermann, *Chem. Sci.*, 2019, **10**, 6584-6593.
16. E. Masson, M. Raeisi and K. Kotturi, *Isr. J. Chem.*, 2018, **58**, 413-434.
17. C. Marquez and W. M. Nau, *Angew. Chem. Int. Ed.*, 2001, **40**, 3155-3160.
18. C. Marquez, R. R. Hudgins and W. M. Nau, *J. Am. Chem. Soc.*, 2004, **126**, 5806-5816.
19. P. Mukhopadhyay, P. Y. Zavalij and L. Isaacs, *J. Am. Chem. Soc.*, 2006, **128**, 14093-14102.
20. Z. Miskolczy, L. Biczok and I. Jablonkai, *Phys. Chem. Chem. Phys.*, 2016, **19**, 766-773.
21. M. H. Tootoonchi, S. Yi and A. E. Kaifer, *J. Am. Chem. Soc.*, 2013, **135**, 10804-10809.
22. H. Tang, D. Fuentealba, Y. H. Ko, N. Selvapalam, K. Kim and C. Bohne, *J. Am. Chem. Soc.*, 2011, **133**, 20623-20633.
23. Z. Miskolczy, J. G. Harangozo, L. Biczok, V. Wintgens, C. Lorthioir and C. Amiel, *Photochem Photobiol Sci*, 2014, **13**, 499-508.
24. S. Senler, B. Cheng and A. E. Kaifer, *Org. Lett.*, 2014, **16**, 5834-5837.
25. B. Held, H. Tang, P. Natarajan, C. P. da Silva, V. de Oliveira Silva, C. Bohne and F. H. Quina, *Photochem Photobiol Sci*, 2016, **15**, 752-757.
26. S. S. Thomas and C. Bohne, *Faraday Discuss.*, 2015, **185**, 381-398.
27. J. Kalmar, S. B. Ellis, M. T. Ashby and R. L. Halterman, *Org. Lett.*, 2012, **14**, 3248-3251.
28. I. Neira, M. D. Garcia, C. Peinador and A. E. Kaifer, *J. Org. Chem.*, 2019, **84**, 2325-2329.
29. S. S. Thomas, H. Tang and C. Bohne, *J. Am. Chem. Soc.*, 2019, **141**, 9645-9654.
30. A. E. Kaifer, W. Li, S. Silvi and V. Sindelar, *Chem Commun (Camb)*, 2012, **48**, 6693-6695.
31. Z. Miskolczy and L. Biczok, *Phys. Chem. Chem. Phys.*, 2014, **16**, 20147-20156.
32. E. A. Appel, F. Biedermann, D. Hoogland, J. Del Barrio, M. D. Driscoll, S. Hay, D. J. Wales and O. A. Scherman, *J. Am. Chem. Soc.*, 2017, **139**, 12985-12993.
33. X. Zheng, Z. Li, M. I. Podariu and D. S. Hage, *Anal. Chem.*, 2014, **86**, 6454-6460.